

B049577

P

6-90-62-98 • NOVEMBER 1962

6-90-62-98

TECHNICAL REPORT: MATERIALS

OXIDATION OF TUNGSTEN AT ULTRA-HIGH TEMPERATURES

Reproduced From  
Best Available Copy

DISTRIBUTION STATEMENT A  
Approved for Public Release  
Distribution Unlimited

PROPERTY OF:  
AMPTIAC LIBRARY

20010914 061

### **NOTICE**

QUALIFIED REQUESTERS MAY OBTAIN COPIES OF THIS REPORT FROM THE ARMED SERVICES TECHNICAL INFORMATION AGENCY (ASTIA). DEPARTMENT OF DEFENSE CONTRACTORS MUST BE ESTABLISHED FOR ASTIA SERVICES, OR HAVE THEIR NEED-TO-KNOW CERTIFIED BY THE MILITARY AGENCY COGNIZANT OF THEIR CONTRACT.

COPIES OF THIS REPORT MAY BE OBTAINED FROM THE OFFICE OF TECHNICAL SERVICES, DEPARTMENT OF COMMERCE, WASHINGTON 25, D.C.

DISTRIBUTION OF THIS REPORT TO OTHERS SHALL NOT BE CONSTRUED AS GRANTING OR IMPLYING A LICENSE TO MAKE, USE, OR SELL ANY INVENTION DESCRIBED HEREIN UPON WHICH A PATENT HAS BEEN GRANTED OR A PATENT APPLICATION FILED BY LOCKHEED AIRCRAFT CORPORATION. NO LIABILITY IS ASSUMED BY LOCKHEED AS TO INFRINGEMENT OF PATENTS OWNED BY OTHERS.

WORK CARRIED OUT AS PART OF THE LOCKHEED INDEPENDENT RESEARCH PROGRAM.

49577

TECHNICAL REPORT: MATERIALS

OXIDATION OF TUNGSTEN AT ULTRA-HIGH TEMPERATURES

by  
R.A. PERKINS  
W.L. PRICE  
D.D. CROOKS

WORK CARRIED OUT AS PART OF THE LOCKHEED INDEPENDENT RESEARCH PROGRAM

*Lockheed*

MISSILES & SPACE COMPANY

A GROUP DIVISION OF LOCKHEED AIRCRAFT CORPORATION

SUNNYVALE, CALIFORNIA

### **NOTICE**

QUALIFIED REQUESTERS MAY OBTAIN COPIES OF THIS REPORT FROM THE ARMED SERVICES TECHNICAL INFORMATION AGENCY (ASTIA). DEPARTMENT OF DEFENSE CONTRACTORS MUST BE ESTABLISHED FOR ASTIA SERVICES, OR HAVE THEIR NEED-TO-KNOW CERTIFIED BY THE MILITARY AGENCY COGNIZANT OF THEIR CONTRACT.

COPIES OF THIS REPORT MAY BE OBTAINED FROM THE OFFICE OF TECHNICAL SERVICES, DEPARTMENT OF COMMERCE, WASHINGTON 25, D.C.

DISTRIBUTION OF THIS REPORT TO OTHERS SHALL NOT BE CONSTRUED AS GRANTING OR IMPLYING A LICENSE TO MAKE, USE, OR SELL ANY INVENTION DESCRIBED HEREIN UPON WHICH A PATENT HAS BEEN GRANTED OR A PATENT APPLICATION FILED BY LOCKHEED AIRCRAFT CORPORATION. NO LIABILITY IS ASSUMED BY LOCKHEED AS TO INFRINGEMENT OF PATENTS OWNED BY OTHERS.

## ABSTRACT

The oxidation behavior of tungsten in air and oxygen has been studied as a function of pressure (0.1 to 5.0 mm Hg) and gas dynamics at temperatures from 1,300 to 3,350°C (2,370 to 6,060°F). The development of a surface recession technique for rate measurement in static and dynamic atmospheres at low pressures is described. Grain size and orientation are shown to influence the rate of oxidation.

Transport of oxygen in the system is a rate-limiting factor in static or turbulent air. Oxygen partial pressure in the reaction chamber varies with the temperature, surface area, and system geometry. High-velocity jet impingement is required to provide a known and constant value of oxygen pressure. Gaseous transport is not rate limiting in pure oxygen at pressures below 3 mm Hg and temperatures to 2,200°C (3,990°F). Identical oxidation rates are obtained by tests in static, turbulent, or high-velocity oxygen and high-velocity air.

Two transitions in oxidation behavior with increasing temperature are observed. A reduction in temperature dependency and an increase in pressure dependency occurs at each transition. At all pressures, rates reach a maximum and decrease with increasing temperature above about 2,200°C (3,990°F). Equations which predict rates of oxidation of tungsten in air and oxygen at pressures of  $10^{-6}$  to 3.0 mm Hg within  $\pm 20$  percent of experimental values from three independent investigations are presented. *End*

## CONTENTS

Section		Page
	ABSTRACT	i
1	INTRODUCTION	1
2	REACTION KINETICS AT HIGH TEMPERATURE	2
3	EXPERIMENTAL	7
	3.1 Materials	7
	3.2 Equipment	7
	3.3 Procedure	9
4	RESULTS	13
	4.1 Rate Reproducibility	13
	4.2 Reactions in Air	17
	4.3 Reactions in Oxygen	22
5	DISCUSSION	27
	5.1 Conclusions	37
6	REFERENCES	39

## TABLES

Table		Page
1	Reproducibility of Oxidation Rates (Turbulent Oxygen)	16
2	Calculated vs Experimental Rates at Low Oxygen Pressure	32

## FIGURES

Figure		Page
1	Oxidation Rate Apparatus	8
2	Pyrometer vs True Temperature Calibration	10
3	Orientation Dependence of Rate at Low Pressure	14
4	Effect of Structure and Composition on Rate Measurements	15
5	Effect of Gas Dynamics on Oxidation Rates in Air	19
6	Comparison of Oxidation Behavior in Air and Oxygen	21
7	Results of Tests from 1300 to 3350°C in Oxygen at 0.11 to 3.0 mm Hg	24
8	Pressure Dependency of Rate in Oxygen	25
9	Comparison of Low-Pressure Oxidation Rate Data	28
10	Pressure Dependency of Maximum Rate of Oxidation	30
11	Temperature-Pressure Relation for Rate Maximum and Transition Points	31
12	Summary of Oxidation Behavior at Low Pressure and High Temperature	36

## Section 1 INTRODUCTION

Serious consideration is being given to the use of tungsten in high-temperature applications above the limits of available protective coating systems. Components capable of operating at temperatures to 3,000°C (5,430°F) are being designed, manufactured, and tested today. Although oxidation-resistant coatings are needed for extended use at high temperatures in air, absolute protection from oxidation is not mandatory for a number of applications. Coatings may not be required where high-temperature exposure occurs at a low partial pressure of oxygen for a relatively short time. For example, uncoated tungsten is used successfully at temperatures approaching its melting point in the nozzles of solid-propellant rocket engines. Although products of combustion contain oxidizing gases, exposure time is of the order of one to two minutes, and loss by oxidation is negligible. Leading edges and heat shields of hypersonic re-entry vehicles will operate at temperatures of 1,200 to 3,000°C (2,190 to 5,430°F). Heating occurs in static and high-velocity air at pressures of  $10^{-4}$  to 20 mm Hg for times of 10 to 100 min (Ref. 1). If surface recession by oxidation under these conditions is small, it can be tolerated by proper design. In some cases, refractory oxide coatings may be used to restrict the access of air and to reduce the oxygen pressure at the metal-oxide interface.

*(7: Follow and also)*

The successful application of this approach to the use of tungsten at ultra-high temperatures demands a precise knowledge of oxidation behavior under the anticipated environmental conditions. [The purpose of this investigation was to obtain rate data for the oxidation of tungsten from 1,300 to 3,400°C (2,370 to 6,150°F) as a function of oxygen pressure and gas dynamics and to obtain an improved understanding of reaction kinetics that will be of theoretical as well as practical utility.]

*back to i  
→ p7*



## Section 2

### REACTION KINETICS AT HIGH TEMPERATURE

There have been only a few investigations of the oxidation of tungsten at temperatures above 1,300°C (2,370°F) and pressures below one atmosphere. Past interest in this subject has been for the use of tungsten as filaments in lamps and electron tubes. Limited data have been obtained for fine-wire and ribbon filaments at temperatures to 2,500°C (4,530°F) in oxygen at pressures of  $10^{-7}$  to  $10^{-2}$  mm Hg. Oxidation data usually are reported in terms of collision efficiency (E), which is defined as the ratio of the rate of removal of oxygen molecules from the surface as  $WO_3$  to the rate of arrival of oxygen at the surface ( $3.5 \times 10^{22} P_{O_2} (32T)^{-1/2}$ ). Rates are expressed as molecules/cm<sup>2</sup>/sec, with  $P_{O_2}$  in mm Hg. These data can be converted to rates of tungsten loss ( $R_W$ ) by the following relations:

$$R_W = 4.275 E P_{O_2} \text{ gm/cm}^2/\text{min} \quad (1)$$

This assumes that the arrival rate of oxygen is a function of pressure and the temperature of the reaction vessel ( $T = 300^\circ K$ ). Langmuir (Ref. 2) has shown that at pressures below  $10^{-2}$  mm Hg, the arrival rate of oxygen at the surface is not perceptibly influenced by the filament temperature.

Langmuir (Ref. 2) conducted the first high-temperature – low-pressure oxidation study in 1913. The rate of clean up of oxygen in a sealed bulb was measured by a pressure-drop technique. The rate of oxidation was found to be a linear function of pressure and an exponential function of temperature. The collision efficiency increased with temperature in the manner of an Arrhenius relation as follows:

$$E = 57.54 \times 10^{-5} \frac{5940}{T} \quad (2)$$

This expression in terms of the rate of tungsten loss expressed in the units of the present work is given by

$$R_W = 256 P_{O_2} \exp. (-27200/RT) - \text{gm/cm}^2/\text{min} \quad (3)$$

Above 927°C (1,700°F), the oxide volatilized without dissociation, leaving the surface clean and bright. At temperatures above 1,500°C (2,730°F), the measured rates were less than those predicted by the Arrhenius equation.

In 1959, Esinger (Ref. 3) reported on the oxidation of tungsten from 927 to 2,127°C (1,700 to 3,860°F) in oxygen at pressures of  $10^{-5}$  to  $10^{-7}$  mm Hg. Collision efficiency was determined by measuring the pumping action of high-purity single-crystal ribbons. Curves of reaction probability versus temperature could be described by the Arrhenius equation at low temperatures but reached a maximum and then decreased with increasing temperature. This behavior was attributed to a decrease in sticking probability of oxygen on tungsten, resulting in reduced probability of oxide formation at high temperature. The low-temperature data agree with those of Langmuir, giving an apparent heat of activation of 25,000 cal/mol. Unlike Langmuir's results, collision efficiency was found to be pressure dependent, and the pressure dependency of rate of oxidation was not linear.

Becker, Becker, and Brandes reported on similar studies in 1961 (Ref. 4). Results of tests from 927 to 2,227°C (1,700 to 4,040°F) in oxygen at pressures from  $10^{-5}$  to  $10^{-7}$  mm Hg were similar to those of Langmuir and Esinger. The collision efficiency was found to increase, pass through a maximum, and then decrease with increasing temperature. This behavior was attributed to changes in the sticking probability and heat of desorption of oxygen on tungsten as a function of temperature. Oxygen was described as adsorbing in two distinct states or layers. For the first layer, the sticking probability (S) was constant at 0.14, with an energy of desorption of 106,000 cal. In the second layer,  $S = 0.04$ , with an energy of desorption of 53,000 cal. Two

rate equations were derived from theoretical considerations and experimental data. In the range from 927 to 1,327°C (1,700 to 2,420°F), the first layer was filled, and the second layer coverage decreased to zero as temperature increased. The collision efficiency is given by

$$E = 60 \times 10^{-\frac{5555}{T}} \quad (4)$$

which converted to the units of this work becomes

$$R_W = 256 P_{O_2} \exp. (-25400/RT) \text{ gm/cm}^2/\text{min} \quad (5)$$

The rate equation is very close to that of Langmuir's, which was obtained by a fit of experimental data to an Arrhenius equation. From 1,727 to 2,127°C (3,140 to 3,860°F) the first layer is partially filled and the coverage decreases to zero with increasing temperature. The rate equation becomes

$$E = 0.11 P_{O_2}^{0.5} 10^{\frac{+6060}{T}} \quad (6)$$

which can be converted to

$$R_W = 0.47 P_{O_2}^{1.5} \exp. (+27700/RT) \text{ gm/cm}^2/\text{min} \quad (7)$$

Thus, at high temperatures, rates are predicted to increase with  $P^{1.5}$ , but to decrease with temperature. Becker et al. also showed that carbon as an impurity in tungsten could accelerate the rate of oxidation by increasing the concentration of adsorbed oxygen on the surface.

The most recent investigation of this phenomenon was conducted by Anderson (Ref. 5) in 1962. Oxidation behavior in the region of the rate maximum was studied from 1,677

to 2,327°C (3,050 to 4,220°F) in oxygen at pressures of  $7.6 \times 10^{-4}$  to  $7.6 \times 10^{-6}$  mm Hg. The results were similar to those found by previous investigators. In the temperature range from 1,877 to 2,327°C (3,410 to 4,220°F), the rate of tungsten loss was observed to increase with  $P_{O_2}^{1.26}$  and to decrease with increasing temperature. Rates were found to depend on the oxygen atom concentration on the surface and varied with pressure to the 1.0 to 1.5 power, depending on surface coverage. Heats of activation were negative and decreased from -14,000 cal to -20,000 cal as pressure decreased.

Only two direct studies of oxidation behavior above 1,300°C (2,370°F) at higher pressures have been reported. Perkins and Crooks (Ref. 6) studied the oxidation of tungsten from 1,300 to 3,000°C (2,370 to 5,430°F) in air at 1 to 15 mm Hg pressure, using a surface recession technique. From 1,300 to 1,700°C (2,370 to 3,090°F), rates could be described by

$$R_W = 14.5 P_{O_2}^{0.62} \exp. (-31500/RT) \text{ gm/cm}^2/\text{min} \quad (8)$$

Oxidation rates reached a maximum at about 1,750°C (3,180°F) and then decreased with increasing temperature. Although the curves resemble those obtained at very low pressures, the rates are considerably less than would be predicted from equations that have been cited. As will be shown, oxygen depletion in the reaction chamber is responsible for the observed behavior, and the measured rates are characteristic of the system, rather than of the material.

Blackburn et al. (Ref. 7), in 1961, reported on the oxidation of tungsten in flowing 21 percent oxygen - 79 percent argon at one atmosphere from 800 to 1,700°C (1,470 to 3,090°F). Rates were determined by oxygen consumption techniques. At temperatures above 1,350°C (2,460°F) the oxide was found to evaporate as fast as it formed. Oxidation rate was found to increase with temperature according to an Arrhenius relation with activation energy of 21,000 cal/mol. The mechanism was assumed to be that

postulated by Langmuir at low pressure; however, the observed rates are considerably less than those which would be predicted by Eqs. (3) or (5).

By considering the oxidation of tungsten as a series of consecutive reactions, Ong (Ref. 8) derived from kinetic theory and experimental data the following rate equation:

$$R_W = 5.89 \times 10^6 P_{O_2}^{0.5} \exp. (-12170/T) \text{ mg/cm}^2/\text{hr} \quad (9)$$

(ATM)

which in terms of this work becomes

$$R_W = 3.56 P_{O_2}^{0.5} \exp. (-24200/RT) \text{ gm/cm}^2/\text{min} \quad (10)$$

(mm)

This equation adequately reproduced rate data from three independent investigations at pressures from 1 mm to 15,800 mm Hg and temperatures from 700 to 1,300°C (1,290 to 2,370°F). Although the temperature-dependent term is similar to that of Eqs. (3) and (5), the pressure-dependent term and constant are significantly different. The rates would be considerably lower than those predicted by other equations. The validity of Eq. (9), however, has not been checked at higher temperatures and lower pressures. Similarly, it is not known if Eqs. (3) and (5) will adequately express rates at pressures above  $10^{-2}$  mm.

One of the objectives of the present work, therefore, is to determine whether a change in mechanism occurs as a function of pressure. The similarity of rate behavior at pressures above 1 mm and below  $10^{-2}$  mm in terms of temperature dependency suggests a common behavior over a wide pressure range. Discrepancies in pressure dependency, however, need to be clarified and resolved. Also, the existence of a maximum in rate versus temperature at pressures above  $10^{-2}$  must be confirmed. A pressure range of  $10^{-1}$  to 5 mm Hg was selected for this study to provide a logical extension of prior work at reduced pressures.

### Section 3

## EXPERIMENTAL

### 3.1 MATERIALS

The tungsten used in this investigation was commercial ground seal rod procured from the General Electric Co. This material, designated as grade MK, is a fine-grain, partially doped tungsten which is 99.95+ percent pure. Principal impurities include C-0.002, O-0.0015, and Mo-0.002 percent. All other impurities are less than 0.001 percent each. The rods were 0.1-in. in diameter by 7-in. long and were centerless ground with a surface finish of 6 to 8. A few tests were made with Grade 218 ground seal rod, which is a fully doped material that is, after heating at high temperature, coarse-grained compared with Grade MK.

Medical Grade tank oxygen 99.96+ percent pure was used in most of the tests. A number of tests were made with Linde Co. Research Grade oxygen, which is 99.99+ percent pure. No effect of impurities in the gas on rates of oxidation was detected. Tests in air were made with normal atmosphere passed through a molecular sieve column. Changes in relative humidity of the air had no discernable effect on rates.

### 3.2 EQUIPMENT

All tests were conducted in a surface recession rate apparatus designed and built by Lockheed Missiles & Space Co. (Fig. 1). Specimens were heated by direct resistance using alternating current at 100 to 300 amp and 5 to 15 v. The rods were positioned vertically in water-cooled electrodes, with slip-fit expansion joints to prevent buckling on heating. A 6-in. diameter by 14-in. high water-cooled, wrought-copper T-section was used for the reaction vessel. Total volume of the system, including pipes and ballast chamber, is about 17 liters. Two sight ports are provided for measurement of temperature and rod diameter. A 1397 B Welch pump and an MCF-300 diffusion pump

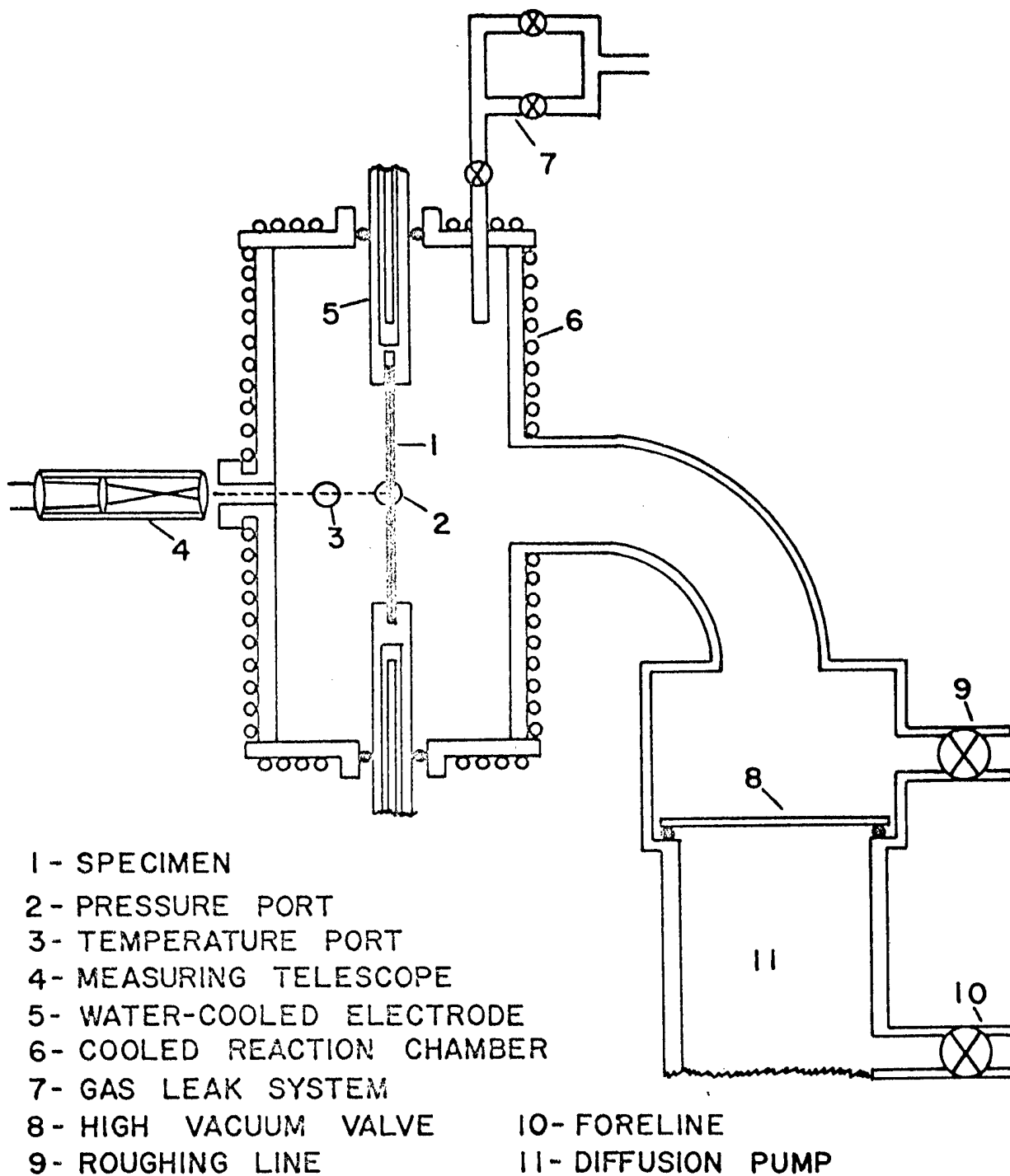


Fig. 1 Oxidation Rate Apparatus

are used in the vacuum system, and an ultimate pressure of  $10^{-5}$  mm Hg with a leak rate of less than 1 micron/min was achieved.

All measurements were made in a plane at the approximate center of the specimen. For most tests, a uniform hot zone, 1 to 2 in. long, existed in the central section of the rod. Temperature was measured with a microoptical pyrometer compensated for emissivity and sight-glass effects (Fig. 2). The pyrometer calibration curve was checked by measuring the apparent melting points of 6 pure metals fastened to the surface of the rod. Further checks were obtained by measuring evaporation rates of tungsten in vacuum, which were compared with published evaporation rate data. The apparent temperature at which the rods melted also was determined for a calibration point. Rod diameters could be measured continuously by means of a filar micrometer eyepiece attached to a 4X telescope having an accuracy of  $\pm 0.0005$  in.

Pressure in the reaction vessel was measured continuously with a Decker Corp. Model 311 Absolute Pressure Meter. The instrument is calibrated from 0.01 to 30 mm in six ranges. Calibration of the gage was checked weekly against a Wallace and Tiernan Model FA 160 Absolute Pressure Meter. This in turn was calibrated every two months against a secondary standard.

### 3.3 PROCEDURE

Tests were conducted in air and oxygen under three different conditions: static, turbulent, and impinging. For static tests, the gas was admitted through a diffuser located in the main vacuum line. The system was pumped continuously and the gas leak rate was balanced against the pumping rate by micrometer leak valves to achieve any desired chamber pressure. This may be viewed as a quasi-static condition in which no measurable degree of turbulence or flow is created in the reaction chamber. Tests in turbulent atmospheres were conducted by admitting the gas leak directly into the reaction chamber while continuously pumping the system. The gas was introduced from a ring manifold concentric with the upper electrode, with jets directed to the chamber



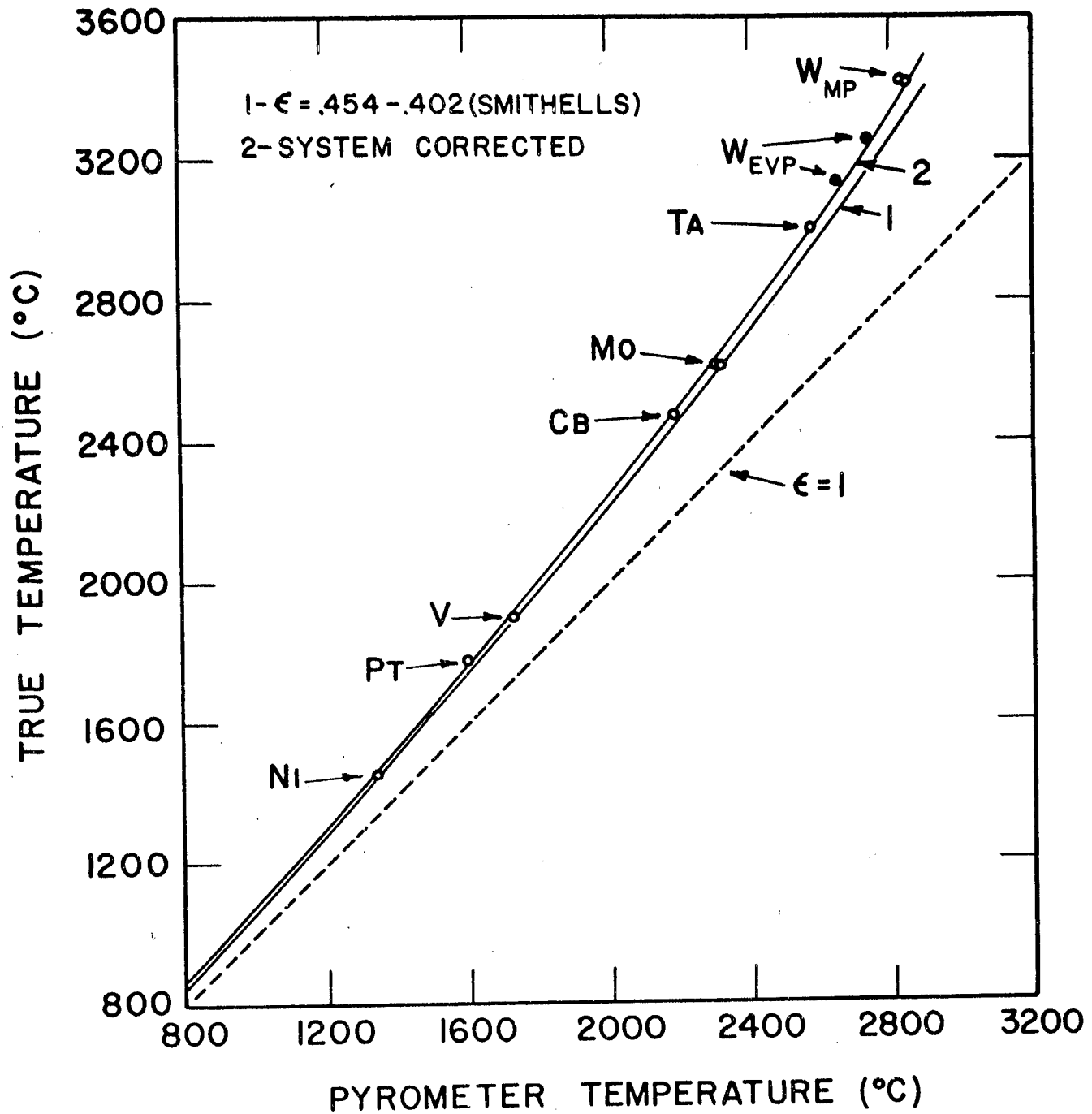


Fig. 2 Pyrometer vs True Temperature Calibration

walls. In high-velocity flow (impinging) tests, gas was admitted from a ring manifold concentric with the specimen near the center line. Twelve jets arranged like the spokes of a wheel were aimed directly at the specimen surface at a distance of about 1/2 inch. Gas leak and pumping rates were adjusted to provide sonic velocity (1140 fps) at the exit plane of each jet. The dynamic pressure versus static chamber pressure was measured to determine gas velocity at the surface of the specimen. This varied from 200 to 900 fps, depending on static chamber pressure. For all impinging tests, the pressure reported is the stagnation (total) pressure of oxygen at the surface.

The normal test procedure was to evacuate the system to less than  $10^{-4}$  mm Hg. and heat the rod for 10 min at 2,000°C (3,630°F). This conditioning treatment was used to degas the system and to provide a uniform metallurgical condition from specimen to specimen. A new specimen was used for each test. After conditioning, the temperature was adjusted to the run temperature and the gas admitted. Approximately 15 sec were required to adjust pressure and temperature to the set values. Zero time was taken at the point when pressure reached about 1/2 the set value. This usually occurred within 5 sec after admitting the gas. At the end of test, the gas leak and power were turned off simultaneously. Final time was taken at the point when pressure had dropped to 1/2 the set value.

[Surface recession at the sight point is one half the difference between initial and final diameters as measured by micrometers.] Rates were calculated by the following relation: -- p17

$$R_W = \frac{49}{t} \frac{(D_o - D_f)}{2} \text{ gm/cm}^2/\text{min} \quad (11)$$

where  $D_o$  and  $D_f$  are initial and final diameters in inches and  $t$  is total time in minutes. This relation also assumes a plane surface and does not take surface roughness into account. All rates are expressed as  $\text{gm/cm}^2/\text{min}$  and can be converted to surface recession in inches/min by dividing by 49. Initially, diameter was measured

continuously by optical telescope and plotted as rate curves to obtain a mean or average rate. However, it was found that surface recession was perfectly linear with time, so that the measurement of initial and final diameter was sufficient to establish an accurate rate. Total time of testing varied from 2 to 60 min, depending on temperature and pressure.

## Section 4

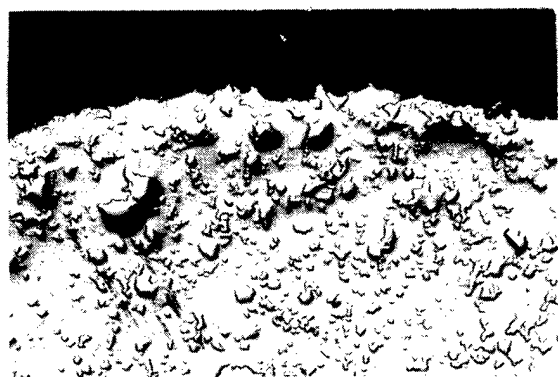
### RESULTS

#### 4.1 RATE REPRODUCIBILITY

Early in the experimental program, it was discovered that oxidation rates varied markedly with crystallographic orientation (Fig. 3). Originally smooth surfaces developed well-defined crystal facets after a few minutes exposure to air or oxygen at high temperature. The extent of faceting was temperature-dependent and tended to become less pronounced on a macro scale at higher temperatures. At temperatures above 2,800°C (5,070°F), mirror finish surfaces often were produced. However, at high magnification even these surfaces were found to be far from smooth (Fig. 3). Cylindrical single-crystal rods formed square cross sections and developed well-defined pyramids on the surface during oxidation at low pressure.

As shown in Fig. 4, this behavior had an effect on the ability to measure rates in an accurate and reproducible manner. The rate of surface recession in  $\text{gm/cm}^2/\text{min}$  is indicated on the figure. For single-crystal rods, rates varied from 0.0235 across the "square" faces to 0.0310 across the "diagonal." For polycrystalline material, the effect results in surface roughening and uneven recession. It becomes particularly difficult to measure recession in coarse-grained tungsten due to the orientation effect. The rate for Grade 218 tungsten, as shown in Fig. 3, varied from 0.0302 to 0.0326, depending on the point of diameter measurement. In fine-grained material, Grade MK, the effect is averaged, and specimens retained a fairly cylindrical cross section with minimum surface roughness. It is for this reason that the type MK fine-grained rod was selected for all test work.

The reproducibility of rate measurements in three different ranges of temperature and pressure for tungsten in turbulent oxygen is shown in Table 1. The two major sources



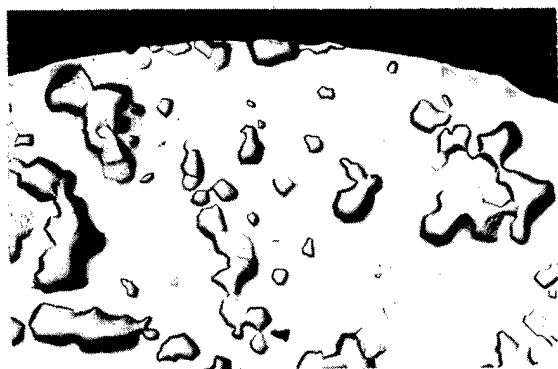
1520 °C

X100



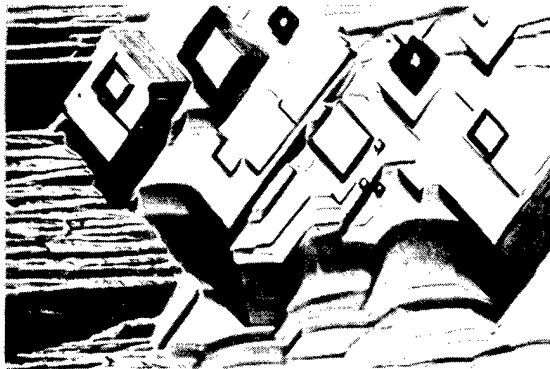
1520 °C

X1000



2100 °C

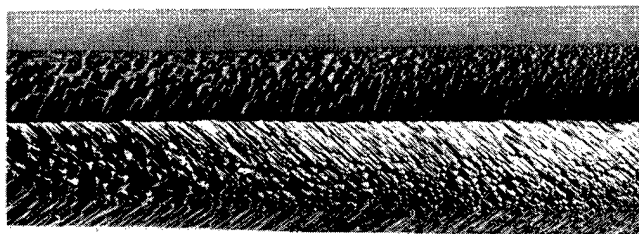
X100



3000 °C

X500

SURFACE



1740 °C - SINGLE CRYSTAL X10

Fig. 3 Orientation Dependence of Rate at Low Pressure

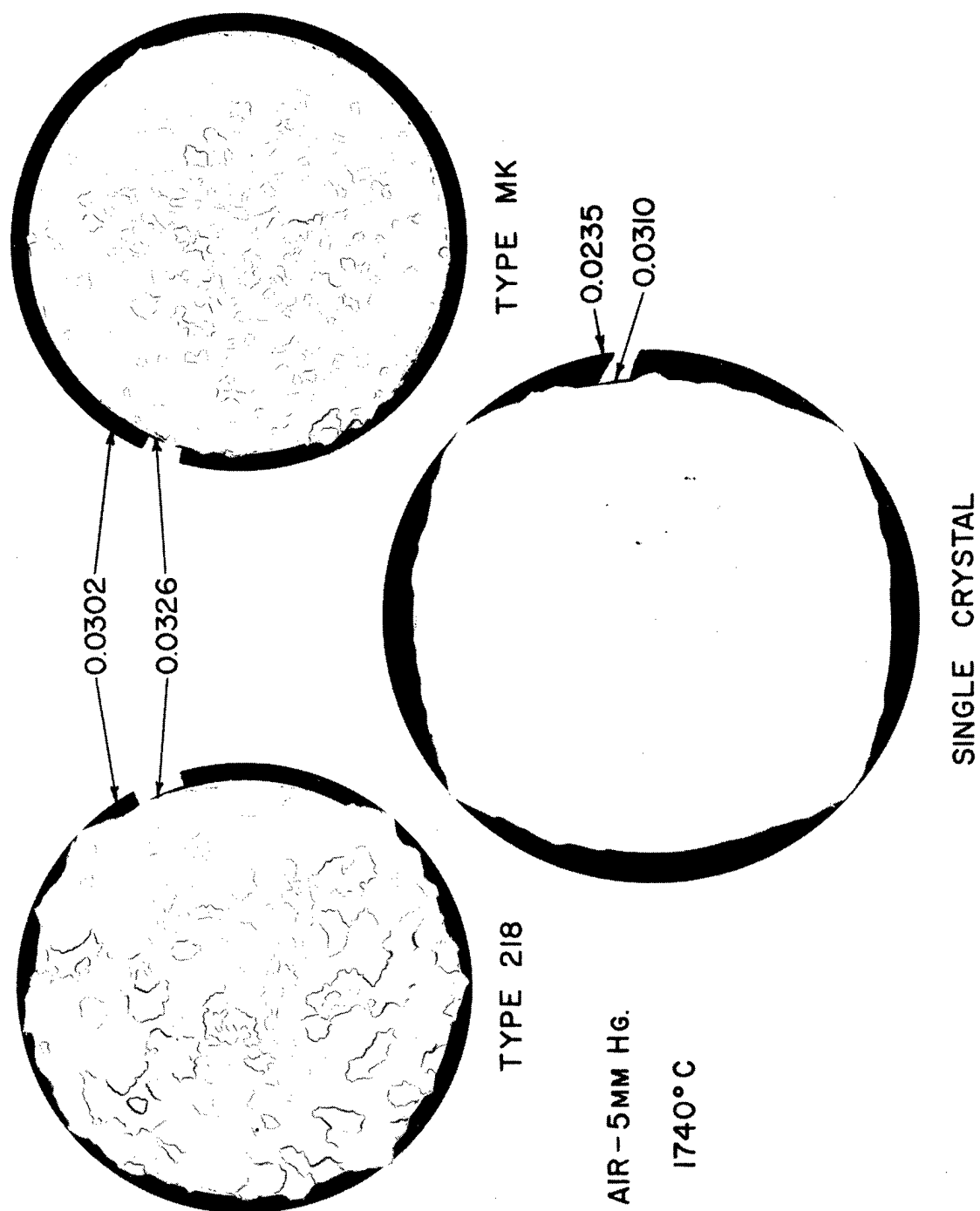


Fig. 4 Effect of Structure and Composition on Rate Measurements

Table 1

## REPRODUCIBILITY OF OXIDATION RATES

1627 °C - 0.22 MM. HG.

DATE -	<u>5/17/62</u>	<u>5/21/62</u>	<u>7/31/62</u>
	0.00717	0.00882	0.00874
		0.00980	0.00923
AVG. -	0.00875 ± 18%	2σ = 20%	

1960 °C - 0.92 MM. HG.

DATE -	<u>7/30/62</u>	<u>9/14/62</u>	<u>9/18/62</u>
	0.0756	0.0716	0.0737
	0.0777		0.0733
	0.0763		
	0.0767		
	0.0765		
AVG. -	0.0752 ± 5%	2σ = 5.2%	

2755 °C - 3.0 MM. HG.

DATE -	<u>6/20/62</u>	<u>9/11/62</u>	<u>9/18/62</u>
	0.465	0.402	0.420
		0.409	
AVG. -	0.424 ± 9.7%	2σ = 11.6%	

of error are in control of specimen temperature and measurement of pressure. The temperature can be measured to within  $\pm 5^\circ\text{C}$  but is difficult to control due to changes in cross section of the rod with time. It is controlled by adjusting the current and tends to drift in an unpredictable manner. This will cause rate variations in consecutive tests as well as in tests conducted at later dates. The effect will be most pronounced in regions where rates are very sensitive to temperature changes. Thus, at  $1,627^\circ\text{C}$  ( $2,960^\circ\text{F}$ ) and 0.22 mm, most of the variation is due to errors in temperature. Pressure, on the other hand, is easy to control within close limits, but the absolute value for any gage reading may vary due to drift in gage calibration. Experience revealed that significant drifts in calibration could occur within the course of several days. At least weekly calibration checks were required to give reproducible data. Consecutive tests proved quite reproducible and errors appeared mostly on a day to day basis. At  $1,960^\circ\text{C}$  ( $3,460^\circ\text{F}$ ) and 0.92 mm, five consecutive runs were reproducible to within  $\pm 1.4$  percent. The day-to-day variation, most likely due to pressure shifts, resulted in a  $\pm 5$  percent reproducibility. [On the average, most rate data were reproducible to  $\pm 10$  percent and were within calculated 2-sigma limits. The greatest variability was found at low temperatures, where rates had a high-temperature dependency.]  $\rightarrow p. 25$

#### 4.2 REACTIONS IN AIR

In order to obtain rate data that could be applied directly to oxidation problems in aerospace structures, initial tests were conducted in static and moving air at low pressure. The preliminary results of this work, which were published in 1961 (Ref. 6), indicated that rates in static air reached a maximum at about  $1,750^\circ\text{C}$  ( $3,180^\circ\text{F}$ ) and then decreased with increasing temperature. This behavior has been studied in more detail at a pressure of 5 mm Hg and found to be the result of oxygen depletion which occurs under static or mildly turbulent conditions.

At the start of oxidation, the tungsten rapidly consumes oxygen, which must be replenished by diffusion or mass transport from the air inlet port. If the system volume is small and the inlet port is remote from the chamber, rates of oxidation can be limited



by transport of oxygen to the reaction chamber. Evidence that this in effect does occur under quasi-static conditions was provided by noting that rate curves were not linear with time for tests beyond 20 to 30 min. As shown in Fig. 5, the slope of the rate curve in static air increased with time. The rate after 60 min of test was almost double that for the initial 10 min of test.

Samples of the atmosphere in the reaction vessel were taken at various time intervals to determine if changing concentration of oxygen was responsible for changes in rate. A gas sample of about 100 ml was drawn into an evacuated bulb and analyzed on a mass spectrometer to determine the ratio of oxygen to nitrogen. These ratios are expressed as percent  $O_2$  in the mixture. Samples were taken from near the surface of the specimen and near the wall of the chamber during test. Analysis of the air before test gave values of 19 to 21 percent  $O_2$ . As shown in Fig. 5, the "air" near the surface of the rod after 5 min of test analyzed 11.9 percent  $O_2$ . Oxygen concentration at the chamber wall was slightly greater but still below normal, indicating that a general depletion of oxygen in the system had occurred. After 30 min, the concentration increased to 14.9 percent, and at the end of one hour it had reached 16.3 percent. Thus, the increase of rate with time is shown to be due to an increase in oxygen concentration with time.

The oxygen content of the atmosphere is governed by a balance between the rate at which the specimen will consume oxygen and the rate at which oxygen can be supplied. If the rate of consumption at a given temperature exceeds the rate of transport in the system, the gas in the chamber is rapidly depleted of oxygen. The rate of consumption then drops until a balance is achieved. Normally, a steady-state condition, where consumption rate equals transport rate, should be reached at some reduced oxygen pressure. However, in this type of test the total surface area and average temperature of the specimen decrease with time. Constant temperature is maintained only at one point on the surface. The total rate of oxygen consumption at any pressure, therefore, will decrease with time, causing a shift in the balance point to higher oxygen pressures. The net effect is an increase in the rate of oxidation at the point of measurement, where temperature is held constant.

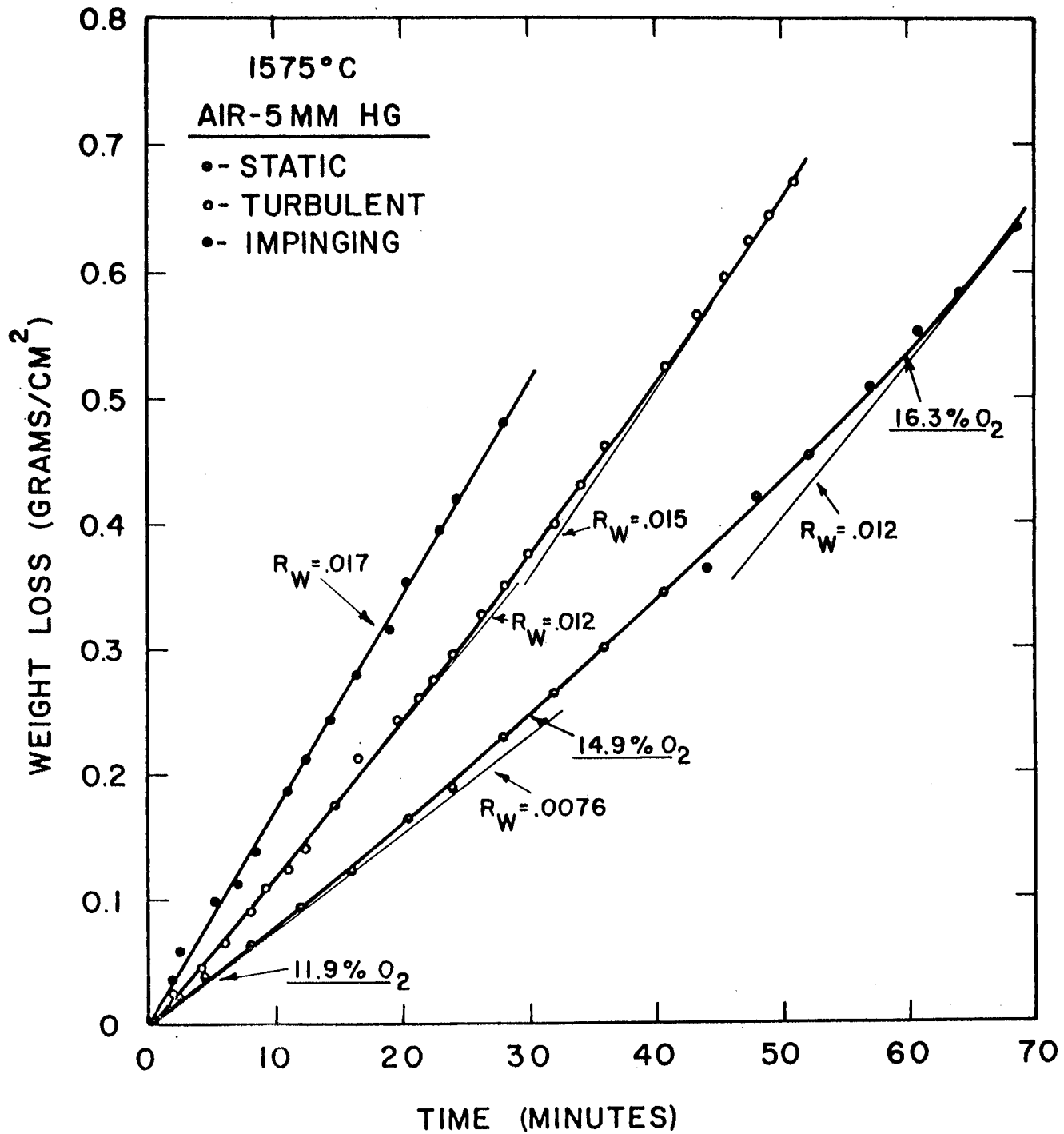


Fig. 5 Effect of Gas Dynamics on Oxidation Rates in Air

If this analysis is correct, then the oxygen concentration in the gas should decrease with increasing specimen temperature. To verify this, samples of the atmosphere were taken for analysis after 4 min of testing at temperatures from 1,350 to 3,000°C (2,460 to 5,430°F). As shown in Fig. 6, oxygen concentration decreased from a high of 19 percent at 1,377°C (2,510°F) to a low of 2.4 percent at 2,590°C (4,690°F).

These data are semi-quantitative and are not an absolute measure of oxygen concentration at the surface. They clearly show, however, that the rate maximum and the decrease in rate with increasing temperature in static air are due to oxygen depletion of the atmosphere. Such rate data are characteristic only of the system and do not reflect the true oxidation behavior of tungsten. For tests in air, it is necessary to increase the rate of transport of oxygen in the system until it is not rate-limiting over the temperature range of interest.

Increased rates of gas transport were achieved by admitting air directly to the reaction chamber to create turbulence and by impinging air on the sample. The results of tests at 5 mm Hg are given in Figs. 5 and 6. The rate of oxidation is significantly increased when turbulence is created; however, depletion of oxygen near the surface still occurs. This is shown by non-linearity of the rate curve and by comparison with impinging-air data. Rates in impinging air were linear with time and were higher than those in turbulent air. At 2,400°C (4,350°F), the impinging air rate was 20 times the static rate and 3 times the turbulent rate.

The rate data in impinging air at 5 mm Hg reveal three different regimes of oxidation behavior with increasing temperature:

- From 1,300 to 1,760°C (2,370 to 3,200°F), rate increased with temperature by an Arrhenius relation with an apparent activation energy of 43,900 cal/mol.
- From 1,760 to 2,630°C (3,200 to 4,770°F), rate increased with temperature by an Arrhenius relation with an apparent activation energy of 24,500 cal/mol.
- Above 2,630°C (4,770°F), rate increased to a maximum at 2,710°C (4,910°F) and then decreased with increasing temperature. The apparent heat of activation decreased to zero and became negative with increasing temperature.

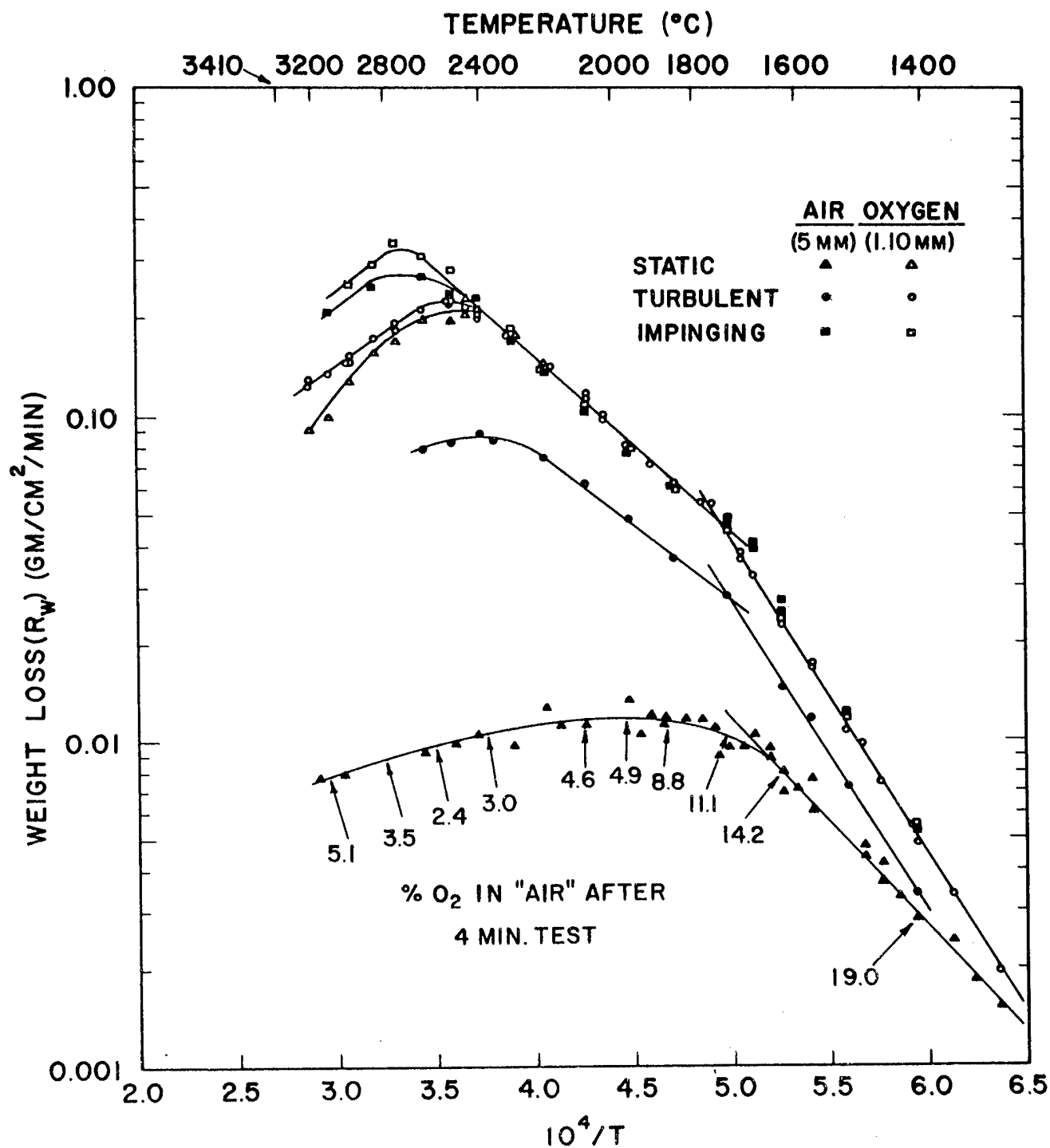


Fig. 6 Comparison of Oxidation Behavior in Air and Oxygen

### 4.3 REACTIONS IN OXYGEN

To further explore the role of gas transport on oxidation behavior and to establish the validity of rates in impinging air, tests were made in static, turbulent, and impinging oxygen at a pressure of 1.1 mm Hg. These data are compared with those from tests in impinging air at 5 mm Hg ( $P_{O_2} = 1.05$  mm) in Fig. 6. At an oxygen pressure of 1.05 to 1.1 mm Hg, the rate of oxidation from 1,300 to 2,350°C (2,370 to 4,260°F) as measured under four different conditions – static, turbulent, and impinging oxygen and impinging air – is identical. Gas velocity up to 900 fps had no measurable effect on kinetics. The data show that under these conditions gaseous transport of reactants and products is not rate-limiting. Data obtained in oxygen can be used directly to predict rates in moving air at velocities approaching Mach 1. Oxygen pressure under dynamic conditions must be taken as the total or stagnation pressure of oxygen at the surface. Although it is believed that no effect of velocity will be found at the higher flow rates characteristic of atmospheric re-entry, extrapolations of the data should be used with a degree of caution.

At oxygen pressures of 1.05 to 1.1 mm Hg and temperatures above 2,300°C (4,170°F), a marked dependency of rates on gas velocity is indicated. In static oxygen, the rate reached a maximum at 2,465°C (4,470°F) and then decreased with rising temperature. In impinging oxygen at 230 fps, the rate maximum was reached at 2,710°C (4,910°F) followed by a similar drop with temperature. Although it is possible that the position of the rate maximum will be shifted to still higher temperatures with increased flow, the data suggest that a limiting condition is being approached. The rate maximum for impinging air ( $v = 900$  fps) occurred at the same temperature as that for impinging oxygen ( $v = 230$  fps) at equivalent oxygen pressures (Fig. 6). The fourfold increase in velocity had little effect and actually resulted in lowered values of oxidation rate.

### 4.4 PRESSURE DEPENDENCY

The pressure dependency of the reaction of tungsten and oxygen was studied from 0.11 to 3.0 mm Hg at 1,300 to 3,350°C (2,370 to 6,060°F), and from 0.10 to 21 mm Hg at

two selected temperatures. As shown in Fig. 7, the curves of log rate versus  $1/T$  have identical form at pressures from 0.11 to 3.0 mm Hg. The curves as drawn represent an average fit of all the data and good agreement of data points with lines of uniform slope at each pressure is shown. The apparent heats of activation are the same as those reported for tests in impinging air: 43,900 cal/mol below the rate transition and 24,500 above. The apparent heats of activation at temperatures above the maximum rate range from -21,100 to -13,800 cal/mol, the slope decreasing with reduced pressure.

Since the slopes in the linear region are parallel for all pressures, the pressure dependency of reaction rate is constant over the temperature range of constant slope. The position of the curves shows that the pressure dependency is higher at temperatures above the rate transition point than at those below. Similarly, pressure dependency beyond the point of maximum rate is higher than that below.

Pressure dependency has been measured for each of these three regions as shown in Fig. 8. A plot of log rate versus log pressure should be linear, with a slope  $N$  equal to the pressure dependency of the reaction. In the low-temperature (high-activation-energy) region, oxidation rate was proportional to oxygen pressure to the 0.59 power. At 1,627°C (2,960°F) in turbulent oxygen, pressure dependency deviated from 0.59 at about 2 to 3 mm Hg and became smaller with increasing pressure. Under impinging conditions, it was constant at 0.59 with increasing pressure to 10 mm Hg. This behavior suggests that transport of reactants or products can be a problem in oxygen atmospheres at pressures above 2 to 3 mm Hg. At 1,627°C (2,960°F) and a pressure of 0.2 mm Hg, the rate transition point is crossed and pressure dependency at lower pressures increased to the value corresponding to that of the second region.

In the second (low-activation-energy) region, pressure dependency at 1,960°C (3,560°F) was constant at 0.82 from 0.1 to 10 mm Hg. The same value was found in turbulent and impinging oxygen. At about 8 mm Hg pressure, the rate transition point is crossed, and pressure dependency at higher pressures will drop to a value of 0.59, which is characteristic of the first region. Thus it can be seen that at constant temperature the

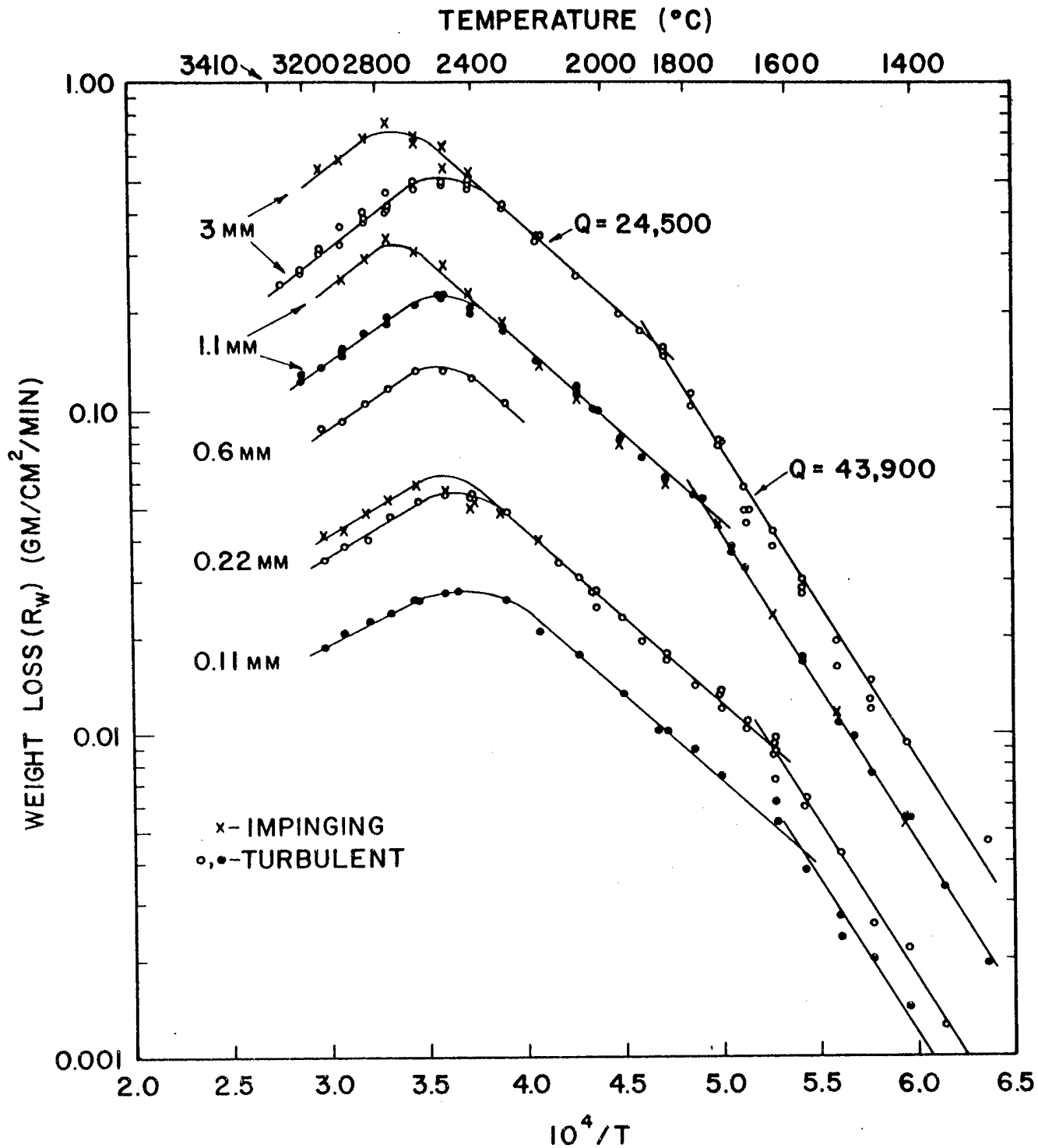


Fig. 7 Results of Tests from 1300 to 3350 $^{\circ}\text{C}$  in Oxygen at 0.11 to 3.0 mm Hg

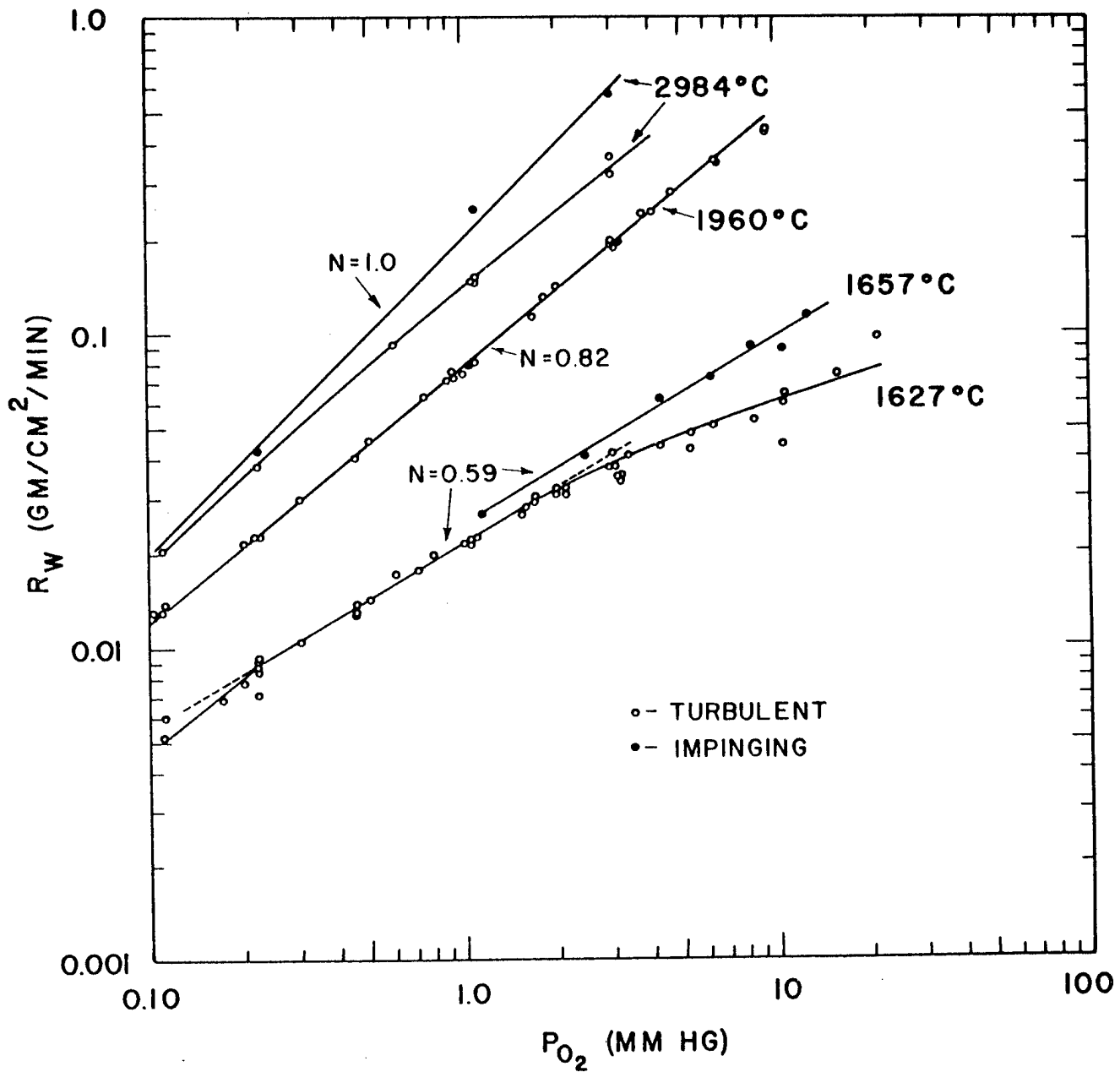


Fig. 8 Pressure Dependency of Rate in Oxygen



dependency of rate on pressure will change whenever the point of rate transition is crossed. This must be taken into account when data are to be extrapolated to higher or lower pressures from any given point.

The pressure dependency at a temperature beyond that of the rate maximum was not constant with pressure under turbulent conditions. At 2,984°C (5,400°F), the value of  $N$  approached 1 at pressures below 0.10 mm and approached 0.8 at a pressure of 1 mm Hg. In impinging oxygen, the value of  $N$  was close to 1.0, indicating a linear dependency on pressure in this region.

## Section 5

### DISCUSSION

There are many similarities between the results of this investigation and those of others conducted at much lower pressures. A graph has been constructed with the data of Esinger (Ref. 3) and Anderson (Ref. 4) to compare the effect of temperature on oxidation rate at oxygen pressures from  $10^{-6}$  to 3.0 mm Hg. (Fig. 9). The low-temperature portion of Esinger's data fits an Arrhenius rate equation with an apparent activation energy of about 25,000 cal/mol. The slope of the second region from our work (24,500 cal/mol) is in excellent agreement with that value. Similar values were reported by Langmuir (Ref. 2) and Becker (Ref. 4). None of the other investigations at low pressure detected the rate transition to a high-activation-energy region at lower temperatures. However, if the temperature for rate transition as determined in this investigation is extrapolated to lower pressures, it can be seen that the other investigations were not conducted at sufficiently low temperatures to detect the break.

One possible exception is the work of Langmuir (Ref. 2), which was conducted at low enough temperatures but in which no break was found. Direct comparison with Langmuir's data may not be valid, however, since the pressure was changing from  $5 \times 10^{-2}$  to  $2 \times 10^{-4}$  mm Hg during his test. All the other studies were made at pressures which were constant or varied over a small range. In order to develop a complete picture of oxidation behavior it will be necessary to study reactions at pressures below  $10^{-1}$  mm Hg in the temperature range where a rate transition would be expected. The existence or absence of such a break will have an important bearing on any mechanistic interpretation of results.

The position and shape of the curves in Fig. 9 suggest a common behavior pattern over the entire range of pressures. If this is true, then it should be possible to correlate the rates and the position of the maximum rate with pressure and temperature. The rate of oxidation at the point of maximum rate for these three independent investigations

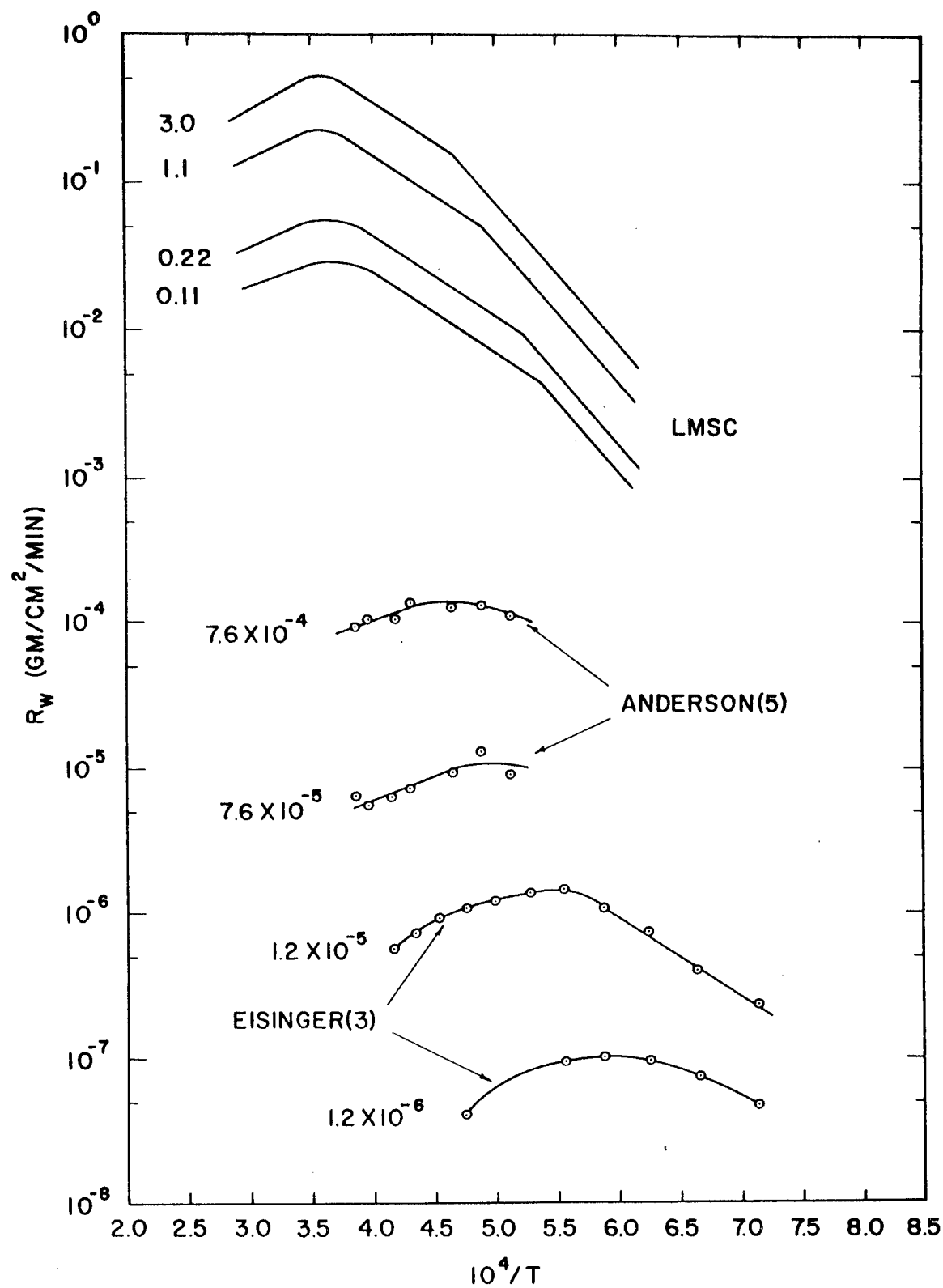


Fig. 9 Comparison of Low-Pressure Oxidation Rate Data

is correlated with oxygen pressure in Fig. 10. The agreement is surprisingly good, considering the very wide range of pressures and rates and the differences in experimental procedure. This correlation shows that the maximum rate of oxidation is close to a linear function of oxygen pressure from  $10^{-6}$  to 1 mm Hg. The maximum rate can be predicted by the following simple relation:

$$R_{\max} = 0.295 P_{O_2}^{1.08} \text{ gm/cm}^2/\text{min} \quad (12)$$

The temperature at which the rate maximum will occur is plotted versus the oxygen pressure in Fig. 11. It can be seen again that an excellent correlation exists between the results of three different investigations. The values from this investigation in turbulent oxygen deviate from the linear relationship at pressures above 0.11 mm Hg. With impingement of oxygen, the point of maximum rate shifted to higher temperature and approached the linear relation. The relation between temperature and pressure for the point of maximum rate can be expressed as follows:

$$P_{O_2} = 2.537 \times 10^7 \exp. (-104000/RT) \quad (13)$$

Further correlation of the results of the three investigations was obtained by the comparison of calculated and experimental rates. By means of an empirical equation fitted to the experimental results of this investigation ( $P_{O_2} = 0.11$  to 3.0 mm Hg), the rate of oxidation was calculated for a point on the linear portion of the log rate versus  $1/T$  curves for five different pressures from  $1.2 \times 10^{-6}$  to 3.0 mm Hg. The results together with values calculated from the equation derived by Becker (Ref. 4) from theoretical considerations are presented in Table 2. An excellent correlation between measured rates and those calculated from the equation derived from our data is shown. Calculated and experimental rates agree with  $\pm 20$  percent over a three-million-fold range of pressure and a  $950^\circ\text{C}$  range of temperature. The magnitude of rates which are accurately predicted varies by a factor of almost ten million. Values calculated from

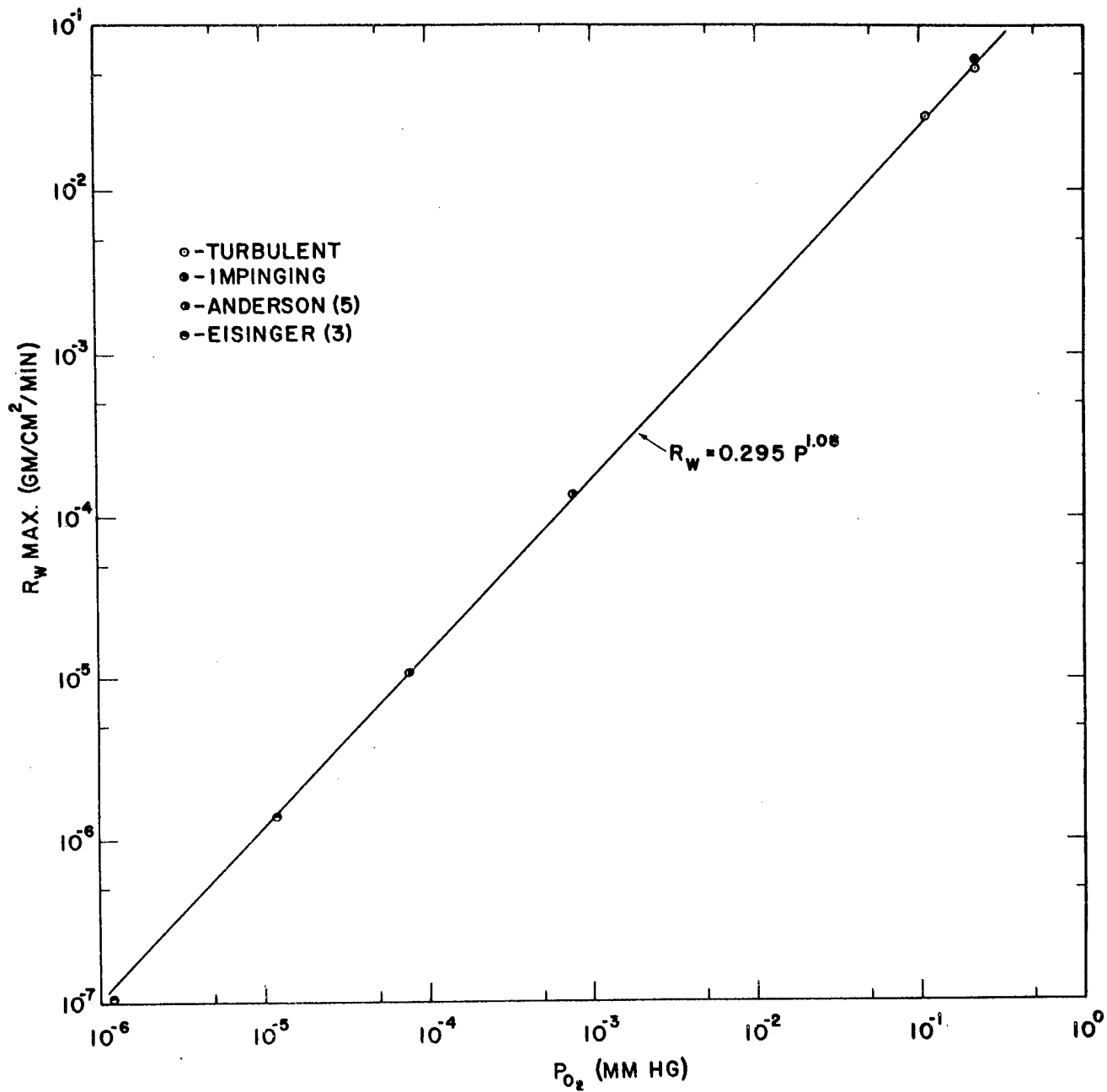


Fig. 10 Pressure Dependency of Maximum Rate of Oxidation

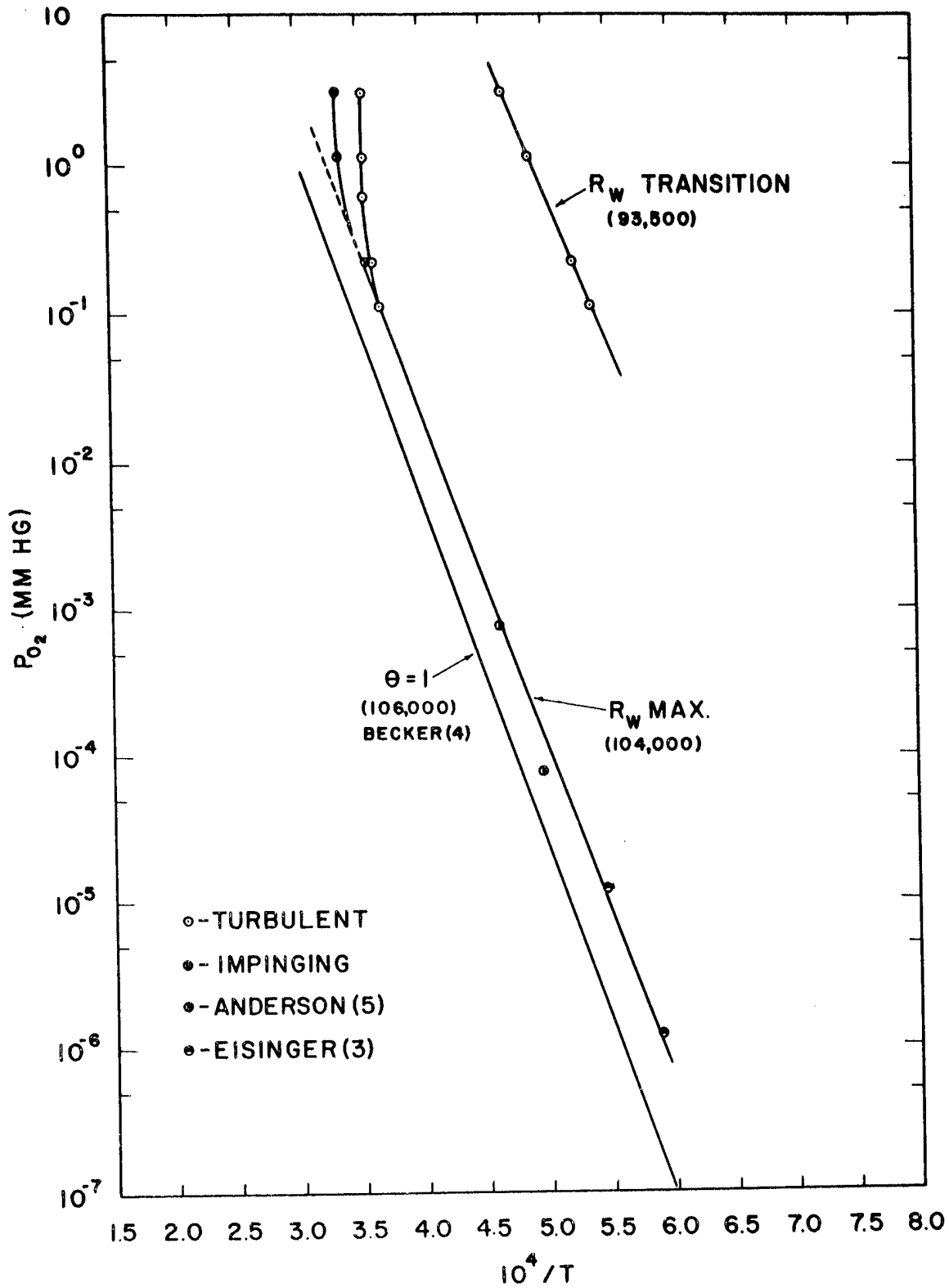


Fig. 11 Temperature-Pressure Relation for Rate Maximum and Transition Points

Table 2

CALCULATED VS EXPERIMENTAL RATES AT LOW OXYGEN PRESSURE

EXPERIMENTAL				CALCULATED	
SOURCE	PRESSURE (MM HG)	TEMPERATURE (°C)	RATE (GM/CM <sup>2</sup> /MIN)	A THIS WORK	B BECKER (4)
THIS WORK	3.0	2077	$2.57 \times 10^{-1}$	$2.63 \times 10^{-1}$	$33.2 \times 10^{-1}$
THIS WORK	$1.1 \times 10^{-1}$	2077	$1.73 \times 10^{-2}$	$1.72 \times 10^{-2}$	$12.2 \times 10^{-2}$
ANDERSON(5)	$7.6 \times 10^{-4}$	1677	$1.10 \times 10^{-4}$	$0.99 \times 10^{-4}$	$2.76 \times 10^{-4}$
EISINGER(3)	$1.2 \times 10^{-5}$	1127	$2.31 \times 10^{-7}$	$2.81 \times 10^{-7}$	$3.31 \times 10^{-7}$
EISINGER(3)	$1.2 \times 10^{-6}$	1127	$4.87 \times 10^{-8}$	$4.18 \times 10^{-8}$	$3.31 \times 10^{-8}$
A) $R_w = 20 P^{0.82} \exp \frac{-24500}{RT}$				B) $R_w = 256 P^{1.0} \exp \frac{-25400}{RT}$	

Becker's equation give fair agreement at low pressure but deviate from measured rates at higher pressure. They are too high by a factor of 10 at pressures of 0.1 to 3.0 mm Hg, although this is reasonable agreement, considering the range of values. Langmuir's (Ref. 2) equation similarly yields an increasingly poor fit with measured rates at increased pressure.

The foregoing comparisons clearly suggest that a common mechanism exists in oxidation of tungsten over an extremely wide range of temperature and pressure. Becker (Ref. 4) has proposed a mechanism based on the fractional coverage of adsorbed oxygen atoms. Atoms are envisioned as chemisorbing in two distinct layers, with the energies of adsorption or desorption being lower in the second layer than in the first. Similarly, the energy of formation and desorption of the oxide is estimated to be lower in the second layer. The transition from two layers to one layer is postulated to occur in the region of the rate maximum. The theory predicts that the rate should decrease with increasing temperature (energy of -27,500 cal/mol) at low coverage ( $\theta < 1$ ) and increase with pressure to the 1.5 power. At high coverage ( $\theta > 1$ ), the rate should increase with temperature (energy of +25,000 cal/mol) and be a linear function of pressure. The relation of pressure and temperature for a monolayer coverage ( $\theta = 1$ ) as derived by Becker is shown in Fig. 11. Good agreement with the curve for the points of maximum rate is indicated. The slope of 106,000 cal/mol is defined by Becker as the heat of adsorption of oxygen on tungsten when the oxygen atom coverage is a monolayer or less.

Although Becker's theory predicts the correct dependence of rate on temperature in the vicinity of the rate maximum, it cannot be accepted as a valid description of reaction mechanism without additional proof. Any mechanistic explanation of the experimental data must be consistent with all aspects of the observed behavior over the entire range of pressure. Specifically, theory must account for the following observations:

- The rate of oxidation is a fractional rather than linear order of oxygen pressure. This fact most likely accounts for the inability of previously derived rate equations to accurately predict rates over a wide range of pressure.



- The temperature and pressure dependency of rate at temperatures below the maximum point change as the temperature is decreased.
- The maximum rate occurs at anomalously low temperatures at high pressures and its position is influenced by gas velocity. (In this case, velocity per se may not be the factor responsible for the change, since increased velocity is accompanied by decreased gas temperature.)
- The rate is dependent on crystal orientation; however, the magnitude of dependence decreases with increased temperature.

The overall problem of developing an adequate mechanistic explanation of observed rate data is complicated by micro and macro faceting of the surface due to orientation effects. Three sources of error result in a significant difference between measured and true rates of the reaction. The surface after a few minutes test resembles a mountain range (Fig. 3). Peaks and valleys are formed as each crystal orientation exposed to the gas assumes its own characteristic rate of recession. On close inspection, it can be seen that the surface consists of a multitude of small plane areas that intersect at well-defined crystallographic angles. Since the amount of metal removed is measured at the peaks, the weight loss is less than the true value by the amount of material which has been removed from the valleys. If the grain size is small and the surface recession large, this difference becomes negligible. A more serious error results from the fact that the measured rate is based on recession of the peaks rather than on recession of the plane faces where the reaction occurs. A geometrical analysis will show that the peak of a pyramid which is growing shorter by recession of its four plane faces will be receding at a faster rate than each face. Thus the measured rate of recession is higher than the true rate of the reaction. The major error results, however, when the rate per unit area is based on an assumed plane surface area which is much smaller than the true surface area exposed to the gas.

The considerations given above imply that when marked faceting of the surface occurs, the measured rate of reaction is significantly larger than the true rate of reaction.

Since the degree of faceting decreases with increasing temperature, significant changes in slope and measured values of activation energy and pressure dependency can occur. This problem has no bearing on the value of the data for engineering purposes. However, if the data are to be used in developing a mechanistic explanation, a serious question as to the validity of calculations can be raised. A study of rate as a function of orientation and true surface area would be helpful in resolving the questions that have been raised. In addition, continuing work on adsorption and desorption, effects of gas temperature and velocity, and identification of oxide vapor species is needed to develop a completely adequate theory.

*the attached chart,*

The results of this investigation are presented in summary form in Fig. 12 and fill a primary need for engineering data for many potential uses of tungsten. They are expressed as equations which define (1) the boundaries where changes in rate behavior occur and (2) the rates of oxidation within each region of uniform behavior as a function of pressure and temperature. A low-temperature boundary that describes the limits for formation of a visible oxide film on tungsten also is presented. Due to a large change in emissivity, it was possible to determine the maximum temperature for any pressure at which solid oxide exists as a visible film or scale on tungsten. The oxide has been tentatively identified as  $W_{18}O_{49}$  by its characteristic red-violet color. This is an important boundary for applications in radiatively cooled structures, since a major change in emissivity occurs. The defining equation is in terms of oxygen pressure; however, in air, the boundary is a function of the total pressure. It is not known whether a change in temperature dependency of rate will occur on crossing this boundary.

The applicability of laboratory test data to performance in operational environments is always an important consideration where marked differences are apparent. The data presented encompass the effects of pressure, temperature, and flow. The range of applicability and limitations of the data have been cited. Two important factors in atmospheric re-entry applications, however, have not been incorporated in this work. These are the gas temperature and molecular dissociation. The gas which strikes the surface of a re-entry structure has been heated to very high temperatures in passing through the shock wave, and the oxygen probably is dissociated. The laboratory studies are based on the reaction of a heated surface with a molecular gas that is close to room

*included  
Fig. 12, 12C,  
P 36.  
Q. 12, 12C,  
12D, 12E,  
12F, 12G,  
12H, 12I,  
12J, 12K,  
12L, 12M,  
12N, 12O,  
12P, 12Q,  
12R, 12S,  
12T, 12U,  
12V, 12W,  
12X, 12Y,  
12Z, 12AA,  
12AB, 12AC,  
12AD, 12AE,  
12AF, 12AG,  
12AH, 12AI,  
12AJ, 12AK,  
12AL, 12AM,  
12AN, 12AO,  
12AP, 12AQ,  
12AR, 12AS,  
12AT, 12AU,  
12AV, 12AW,  
12AX, 12AY,  
12AZ, 12BA,  
12BB, 12BC,  
12BD, 12BE,  
12BF, 12BG,  
12BH, 12BI,  
12BJ, 12BK,  
12BL, 12BM,  
12BN, 12BO,  
12BP, 12BQ,  
12BR, 12BS,  
12BT, 12BU,  
12BV, 12BW,  
12BX, 12BY,  
12BZ, 12CA,  
12CB, 12CC,  
12CD, 12CE,  
12CF, 12CG,  
12CH, 12CI,  
12CJ, 12CK,  
12CL, 12CM,  
12CN, 12CO,  
12CP, 12CQ,  
12CR, 12CS,  
12CT, 12CU,  
12CV, 12CW,  
12CX, 12CY,  
12CZ, 12DA,  
12DB, 12DC,  
12DD, 12DE,  
12DF, 12DG,  
12DH, 12DI,  
12DJ, 12DK,  
12DL, 12DM,  
12DN, 12DO,  
12DP, 12DQ,  
12DR, 12DS,  
12DT, 12DU,  
12DV, 12DW,  
12DX, 12DY,  
12DZ, 12EA,  
12EB, 12EC,  
12ED, 12EE,  
12EF, 12EG,  
12EH, 12EI,  
12EJ, 12EK,  
12EL, 12EM,  
12EN, 12EO,  
12EP, 12EQ,  
12ER, 12ES,  
12ET, 12EU,  
12EV, 12EW,  
12EX, 12EY,  
12EZ, 12FA,  
12FB, 12FC,  
12FD, 12FE,  
12FF, 12FG,  
12FH, 12FI,  
12FJ, 12FK,  
12FL, 12FM,  
12FN, 12FO,  
12FP, 12FQ,  
12FR, 12FS,  
12FT, 12FU,  
12FV, 12FW,  
12FX, 12FY,  
12FZ, 12GA,  
12GB, 12GC,  
12GD, 12GE,  
12GF, 12GG,  
12GH, 12GI,  
12GJ, 12GK,  
12GL, 12GM,  
12GN, 12GO,  
12GP, 12GQ,  
12GR, 12GS,  
12GT, 12GU,  
12GV, 12GW,  
12GX, 12GY,  
12GZ, 12HA,  
12HB, 12HC,  
12HD, 12HE,  
12HF, 12HG,  
12HH, 12HI,  
12HJ, 12HK,  
12HL, 12HM,  
12HN, 12HO,  
12HP, 12HQ,  
12HR, 12HS,  
12HT, 12HU,  
12HV, 12HW,  
12HX, 12HY,  
12HZ, 12IA,  
12IB, 12IC,  
12ID, 12IE,  
12IF, 12IG,  
12IH, 12II,  
12IJ, 12IK,  
12IL, 12IM,  
12IN, 12IO,  
12IP, 12IQ,  
12IR, 12IS,  
12IT, 12IU,  
12IV, 12IW,  
12IX, 12IY,  
12IZ, 12JA,  
12JB, 12JC,  
12JD, 12JE,  
12JF, 12JG,  
12JH, 12JI,  
12JJ, 12JK,  
12JL, 12JM,  
12JN, 12JO,  
12JP, 12JQ,  
12JR, 12JS,  
12JT, 12JU,  
12JV, 12JW,  
12JX, 12JY,  
12JZ, 12KA,  
12KB, 12KC,  
12KD, 12KE,  
12KF, 12KG,  
12KH, 12KI,  
12KJ, 12KK,  
12KL, 12KM,  
12KN, 12KO,  
12KP, 12KQ,  
12KR, 12KS,  
12KT, 12KU,  
12KV, 12KW,  
12KX, 12KY,  
12KZ, 12LA,  
12LB, 12LC,  
12LD, 12LE,  
12LF, 12LG,  
12LH, 12LI,  
12LJ, 12LK,  
12LL, 12LM,  
12LN, 12LO,  
12LP, 12LQ,  
12LR, 12LS,  
12LT, 12LU,  
12LV, 12LW,  
12LX, 12LY,  
12LZ, 12MA,  
12MB, 12MC,  
12MD, 12ME,  
12MF, 12MG,  
12MH, 12MI,  
12MJ, 12MK,  
12ML, 12MM,  
12MN, 12MO,  
12MP, 12MQ,  
12MR, 12MS,  
12MT, 12MU,  
12MV, 12MW,  
12MX, 12MY,  
12MZ, 12NA,  
12NB, 12NC,  
12ND, 12NE,  
12NF, 12NG,  
12NH, 12NI,  
12NJ, 12NK,  
12NL, 12NM,  
12NN, 12NO,  
12NP, 12NQ,  
12NR, 12NS,  
12NT, 12NU,  
12NV, 12NW,  
12NX, 12NY,  
12NZ, 12OA,  
12OB, 12OC,  
12OD, 12OE,  
12OF, 12OG,  
12OH, 12OI,  
12OJ, 12OK,  
12OL, 12OM,  
12ON, 12OO,  
12OP, 12OQ,  
12OR, 12OS,  
12OT, 12OU,  
12OV, 12OW,  
12OX, 12OY,  
12OZ, 12PA,  
12PB, 12PC,  
12PD, 12PE,  
12PF, 12PG,  
12PH, 12PI,  
12PJ, 12PK,  
12PL, 12PM,  
12PN, 12PO,  
12PP, 12PQ,  
12PR, 12PS,  
12PT, 12PU,  
12PV, 12PW,  
12PX, 12PY,  
12PZ, 12QA,  
12QB, 12QC,  
12QD, 12QE,  
12QF, 12QG,  
12QH, 12QI,  
12QJ, 12QK,  
12QL, 12QM,  
12QN, 12QO,  
12QP, 12QQ,  
12QR, 12QS,  
12QT, 12QU,  
12QV, 12QW,  
12QX, 12QY,  
12QZ, 12RA,  
12RB, 12RC,  
12RD, 12RE,  
12RF, 12RG,  
12RH, 12RI,  
12RJ, 12RK,  
12RL, 12RM,  
12RN, 12RO,  
12RP, 12RQ,  
12RR, 12RS,  
12RT, 12RU,  
12RV, 12RW,  
12RX, 12RY,  
12RZ, 12SA,  
12SB, 12SC,  
12SD, 12SE,  
12SF, 12SG,  
12SH, 12SI,  
12SJ, 12SK,  
12SL, 12SM,  
12SN, 12SO,  
12SP, 12SQ,  
12SR, 12SS,  
12ST, 12SU,  
12SV, 12SW,  
12SX, 12SY,  
12SZ, 12TA,  
12TB, 12TC,  
12TD, 12TE,  
12TF, 12TG,  
12TH, 12TI,  
12TJ, 12TK,  
12TL, 12TM,  
12TN, 12TO,  
12TP, 12TQ,  
12TR, 12TS,  
12TT, 12TU,  
12TV, 12TW,  
12TX, 12TY,  
12TZ, 12UA,  
12UB, 12UC,  
12UD, 12UE,  
12UF, 12UG,  
12UH, 12UI,  
12UJ, 12UK,  
12UL, 12UM,  
12UN, 12UO,  
12UP, 12UQ,  
12UR, 12US,  
12UT, 12UU,  
12UV, 12UW,  
12UX, 12UY,  
12UZ, 12VA,  
12VB, 12VC,  
12VD, 12VE,  
12VF, 12VG,  
12VH, 12VI,  
12VJ, 12VK,  
12VL, 12VM,  
12VN, 12VO,  
12VP, 12VQ,  
12VR, 12VS,  
12VT, 12VU,  
12VV, 12VW,  
12VX, 12VY,  
12VZ, 12WA,  
12WB, 12WC,  
12WD, 12WE,  
12WF, 12WG,  
12WH, 12WI,  
12WJ, 12WK,  
12WL, 12WM,  
12WN, 12WO,  
12WP, 12WQ,  
12WR, 12WS,  
12WT, 12WU,  
12WV, 12WW,  
12WX, 12WY,  
12WZ, 12XA,  
12XB, 12XC,  
12XD, 12XE,  
12XF, 12XG,  
12XH, 12XI,  
12XJ, 12XK,  
12XL, 12XM,  
12XN, 12XO,  
12XP, 12XQ,  
12XR, 12XS,  
12XT, 12XU,  
12XV, 12XW,  
12XX, 12XY,  
12XZ, 12YA,  
12YB, 12YC,  
12YD, 12YE,  
12YF, 12YG,  
12YH, 12YI,  
12YJ, 12YK,  
12YL, 12YM,  
12YN, 12YO,  
12YP, 12YQ,  
12YR, 12YS,  
12YT, 12YU,  
12YV, 12YW,  
12YX, 12YY,  
12YZ, 12ZA,  
12ZB, 12ZC,  
12ZD, 12ZE,  
12ZF, 12ZG,  
12ZH, 12ZI,  
12ZJ, 12ZK,  
12ZL, 12ZM,  
12ZN, 12ZO,  
12ZP, 12ZQ,  
12ZR, 12ZS,  
12ZT, 12ZU,  
12ZV, 12ZW,  
12ZX, 12ZY,  
12ZZ, 12AA,  
12AB, 12AC,  
12AD, 12AE,  
12AF, 12AG,  
12AH, 12AI,  
12AJ, 12AK,  
12AL, 12AM,  
12AN, 12AO,  
12AP, 12AQ,  
12AR, 12AS,  
12AT, 12AU,  
12AV, 12AW,  
12AX, 12AY,  
12AZ, 12BA,  
12BB, 12BC,  
12BD, 12BE,  
12BF, 12BG,  
12BH, 12BI,  
12BJ, 12BK,  
12BL, 12BM,  
12BN, 12BO,  
12BP, 12BQ,  
12BR, 12BS,  
12BT, 12BU,  
12BV, 12BW,  
12BX, 12BY,  
12BZ, 12CA,  
12CB, 12CC,  
12CD, 12CE,  
12CF, 12CG,  
12CH, 12CI,  
12CJ, 12CK,  
12CL, 12CM,  
12CN, 12CO,  
12CP, 12CQ,  
12CR, 12CS,  
12CT, 12CU,  
12CV, 12CW,  
12CX, 12CY,  
12CZ, 12DA,  
12DB, 12DC,  
12DD, 12DE,  
12DF, 12DG,  
12DH, 12DI,  
12DJ, 12DK,  
12DL, 12DM,  
12DN, 12DO,  
12DP, 12DQ,  
12DR, 12DS,  
12DT, 12DU,  
12DV, 12DW,  
12DX, 12DY,  
12DZ, 12EA,  
12EB, 12EC,  
12ED, 12EE,  
12EF, 12EG,  
12EH, 12EI,  
12EJ, 12EK,  
12EL, 12EM,  
12EN, 12EO,  
12EP, 12EQ,  
12ER, 12ES,  
12ET, 12EU,  
12EV, 12EW,  
12EX, 12EY,  
12EZ, 12FA,  
12FB, 12FC,  
12FD, 12FE,  
12FF, 12FG,  
12FH, 12FI,  
12FJ, 12FK,  
12FL, 12FM,  
12FN, 12FO,  
12FP, 12FQ,  
12FR, 12FS,  
12FT, 12FU,  
12FV, 12FW,  
12FX, 12FY,  
12FZ, 12GA,  
12GB, 12GC,  
12GD, 12GE,  
12GF, 12GG,  
12GH, 12GI,  
12GJ, 12GK,  
12GL, 12GM,  
12GN, 12GO,  
12GP, 12GQ,  
12GR, 12GS,  
12GT, 12GU,  
12GV, 12GW,  
12GX, 12GY,  
12GZ, 12HA,  
12HB, 12HC,  
12HD, 12HE,  
12HF, 12HG,  
12HH, 12HI,  
12HJ, 12HK,  
12HL, 12HM,  
12HN, 12HO,  
12HP, 12HQ,  
12HR, 12HS,  
12HT, 12HU,  
12HV, 12HW,  
12HX, 12HY,  
12HZ, 12IA,  
12IB, 12IC,  
12ID, 12IE,  
12IF, 12IG,  
12IH, 12II,  
12IJ, 12IK,  
12IL, 12IM,  
12IN, 12IO,  
12IP, 12IQ,  
12IR, 12IS,  
12IT, 12IU,  
12IV, 12IW,  
12IX, 12IY,  
12IZ, 12JA,  
12JB, 12JC,  
12JD, 12JE,  
12JF, 12JG,  
12JH, 12JI,  
12JJ, 12JK,  
12JL, 12JM,  
12JN, 12JO,  
12JP, 12JQ,  
12JR, 12JS,  
12JT, 12JU,  
12JV, 12JW,  
12JX, 12JY,  
12JZ, 12KA,  
12KB, 12KC,  
12KD, 12KE,  
12KF, 12KG,  
12KH, 12KI,  
12KJ, 12KK,  
12KL, 12KM,  
12KN, 12KO,  
12KP, 12KQ,  
12KR, 12KS,  
12KT, 12KU,  
12KV, 12KW,  
12KX, 12KY,  
12KZ, 12LA,  
12LB, 12LC,  
12LD, 12LE,  
12LF, 12LG,  
12LH, 12LI,  
12LJ, 12LK,  
12LL, 12LM,  
12LN, 12LO,  
12LP, 12LP,  
12LR, 12LS,  
12LT, 12LU,  
12LV, 12LV,  
12LX, 12LY,  
12LZ, 12MA,  
12MB, 12MC,  
12MD, 12ME,  
12MF, 12MF,  
12MH, 12MH,  
12MI, 12MI,  
12MJ, 12MJ,  
12MK, 12MK,  
12ML, 12ML,  
12MN, 12MN,  
12MO, 12MO,  
12MP, 12MP,  
12MQ, 12MQ,  
12MR, 12MR,  
12MS, 12MS,  
12MT, 12MT,  
12MU, 12MU,  
12MV, 12MV,  
12MW, 12MW,  
12MX, 12MX,  
12MY, 12MY,  
12MZ, 12MZ,  
12NA, 12NA,  
12NB, 12NB,  
12NC, 12NC,  
12ND, 12ND,  
12NE, 12NE,  
12NF, 12NF,  
12NG, 12NG,  
12NH, 12NH,  
12NI, 12NI,  
12NJ, 12NJ,  
12NK, 12NK,  
12NL, 12NL,  
12NM, 12NM,  
12NO, 12NO,  
12NP, 12NP,  
12NQ, 12NQ,  
12NR, 12NR,  
12NS, 12NS,  
12NT, 12NT,  
12NU, 12NU,  
12NV, 12NV,  
12NW, 12NW,  
12NX, 12NX,  
12NY, 12NY,  
12NZ, 12NZ,  
12OA, 12OA,  
12OB, 12OB,  
12OC, 12OC,  
12OD, 12OD,  
12OE, 12OE,  
12OF, 12OF,  
12OG, 12OG,  
12OH, 12OH,  
12OI, 12OI,  
12OJ, 12OJ,  
12OK, 12OK,  
12OL, 12OL,  
12OM, 12OM,  
12ON, 12ON,  
12OO, 12OO,  
12OP, 12OP,  
12OQ, 12OQ,  
12OR, 12OR,  
12OS, 12OS,  
12OT, 12OT,  
12OU, 12OU,  
12OV, 12OV,  
12OW, 12OW,  
12OX, 12OX,  
12OY, 12OY,  
12OZ, 12OZ,  
12PA, 12PA,  
12PB, 12PB,  
12PC, 12PC,  
12PD, 12PD,  
12PE, 12PE,  
12PF, 12PF,  
12PG, 12PG,  
12PH, 12PH,  
12PI, 12PI,  
12PJ, 12PJ,  
12PK, 12PK,  
12PL, 12PL,  
12PM, 12PM,  
12PN, 12PN,  
12PO, 12PO,  
12PP, 12PP,  
12PQ, 12PQ,  
12PR, 12PR,  
12PS, 12PS,  
12PT, 12PT,  
12PU, 12PU,  
12PV, 12PV,  
12PW, 12PW,  
12PX, 12PX,  
12PY, 12PY,  
12PZ, 12PZ,  
12QA, 12QA,  
12QB, 12QB,  
12QC, 12QC,  
12QD, 12QD,  
12QE, 12QE,  
12QF, 12QF,  
12QG, 12QG,  
12QH, 12QH,  
12QI, 12QI,  
12QJ, 12QJ,  
12QK, 12QK,  
12QL, 12QL,  
12QM, 12QM,  
12QN, 12QN,  
12QO, 12QO,  
12QP, 12QP,  
12QQ, 12QQ,  
12QR, 12QR,  
12QS, 12QS,  
12QT, 12QT,  
12QU, 12QU,  
12QV, 12QV,  
12QW, 12QW,  
12QX, 12QX,  
12QY, 12QY,  
12QZ, 12QZ,  
12RA, 12RA,  
12RB, 12RB,  
12RC, 12RC,  
12RD, 12RD,  
12RE, 12RE,  
12RF, 12RF,  
12RG, 12RG,  
12RH, 12RH,  
12RI, 12RI,  
12RJ, 12RJ,  
12RK, 12RK,  
12RL, 12RL,  
12RM, 12RM,  
12RN, 12RN,  
12RO, 12RO,  
12RP, 12RP,  
12RQ, 12RQ,  
12RR, 12RR,  
12RS, 12RS,  
12RT, 12RT,  
12RU, 12RU,  
12RV, 12RV,  
12RW, 12RW,  
12RX, 12RX,  
12RY, 12RY,  
12RZ, 12RZ,  
12SA, 12SA,  
12SB, 12SB,  
12SC, 12SC,  
12SD, 12SD,  
12SE, 12SE,  
12SF, 12SF,  
12SG, 12SG,  
12SH, 12SH,  
12SI, 12SI,  
12SJ, 12SJ,  
12SK, 12SK,  
12SL, 12SL,  
12SM, 12SM,  
12SN, 12SN,  
12SO, 12SO,  
12SP, 12SP,  
12SQ, 12SQ,  
12SR, 12SR,  
12SS, 12SS,  
12ST, 12ST,  
12SU, 12SU,  
12SV, 12SV,  
12SW, 12SW,  
12SX, 12SX,  
12SY, 12SY,  
12SZ, 12SZ,  
12TA, 12TA,  
12TB, 12TB,  
12TC, 12TC,  
12TD, 12TD,  
12TE, 12TE,  
12TF, 12TF,  
12TG, 12TG,  
12TH, 12TH,  
12TI, 12TI,  
12TJ, 12TJ,  
12TK, 12TK,  
12TL, 12TL,  
12TM, 12TM,  
12TN, 12TN,  
12TO, 12TO,  
12TP, 12TP,  
12TQ, 12TQ,  
12TR, 12TR,  
12TS, 12TS,  
12TT, 12TT,  
12TU, 12TU,  
12TV, 12TV,  
12TW, 12TW,  
12TX, 12TX,  
12TY, 12TY,  
12TZ, 12TZ,  
12UA, 12UA,  
12UB, 12UB,  
12UC, 12UC,  
12UD, 12UD,  
12UE, 12UE,  
12UF, 12UF,  
12UG, 12UG,  
12UH, 12UH,  
12UI, 12UI,  
12UJ, 12UJ,  
12UK, 12UK,  
12UL, 12UL,  
12UM, 12UM,  
12UN, 12UN,  
12UO, 12UO,  
12UP, 12UP,  
12UQ, 12UQ,  
12UR, 12UR,  
12US, 12US,  
12UT, 12UT,  
12UU, 12UU,  
12UV, 12UV,  
12UW, 12UW,  
12UX, 12UX,  
12UY, 12UY,  
12UZ, 12UZ,  
12VA, 12VA,  
12VB, 12VB,  
12VC, 12VC,  
12VD, 12VD,  
12VE, 12VE,  
12VF, 12VF,  
12VG, 12VG,  
12VH, 12VH,  
12VI, 12VI,  
12VJ, 12VJ,  
12VK, 12VK,  
12VL, 12VL,  
12VM, 12VM,  
12VN, 12VN,  
12VO, 12VO,  
12VP, 12VP,  
12VQ, 12VQ,  
12VR, 12VR,  
12VS, 12VS,  
12VT, 12VT,  
12VU, 12VU,  
12VV, 12VV,  
12VW, 12VW,  
12VX, 12VX,  
12VY, 12VY,  
12VZ, 12VZ,  
12WA, 12WA,  
12WB, 12WB,  
12WC, 12WC,  
12WD, 12WD,  
12WE, 12WE,  
12WF, 12WF,  
12WG, 12WG,  
12WH, 12WH,  
12WI, 12WI,  
12WJ, 12WJ,  
12WK, 12WK,  
12WL, 12WL,  
12WM, 12WM,  
12WN, 12WN,  
12WO, 12WO,  
12WP, 12WP,  
12WQ, 12WQ,  
12WR, 12WR,  
12WS, 12WS,  
12WT, 12WT,  
12WU, 12WU,  
12WV, 12WV,  
12WW, 12WW,  
12WX, 12WX,  
12WY, 12WY,  
12WZ, 12WZ,  
12XA, 12XA,  
12XB, 12XB,  
12XC, 12XC,  
12XD, 12XD,  
12XE, 12XE,  
12XF, 12XF,  
12XG, 12XG,  
12XH, 12XH,  
12XI, 12XI,  
12XJ, 12XJ,  
12XK, 12XK,  
12XL, 12XL,  
12XM, 12XM,  
12XN, 12XN,  
12XO, 12XO,  
12XP, 12XP,  
12XQ, 12XQ,  
12XR, 12XR,  
12XS, 12XS,  
12XT, 12XT,  
12XU, 12XU,  
12XV, 12XV,  
12XW, 12XW,  
12XX, 12XX,  
12XY, 12XY,  
12XZ, 12XZ,  
12YA, 12YA,  
12YB, 12YB,  
12YC, 12YC,  
12YD, 12YD,  
12YE, 12YE,  
12YF, 12YF,  
12YG, 12YG,  
12YH, 12YH,  
12YI, 12YI,  
12YJ, 12YJ,  
12YK, 12YK,  
12YL, 12YL,  
12YM, 12YM,  
12YN, 12YN,  
12YO, 12YO,  
12YP, 12YP,  
12YQ, 12YQ,  
12YR, 12YR,  
12YS, 12YS,  
12YT, 12YT,  
12YU, 12YU,  
12YV, 12YV,  
12YW, 12YW,  
12YX, 12YX,  
12YY, 12YY,  
12YZ, 12YZ,  
12ZA, 12ZA,  
12ZB, 12ZB,  
12ZC, 12ZC,  
12ZD, 12ZD,  
12ZE, 12ZE,  
12ZF, 12ZF,  
12ZG, 12ZG,  
12ZH, 12ZH,  
12ZI, 12ZI,  
12ZJ, 12ZJ,  
12ZK, 12ZK,  
12ZL, 12ZL,  
12ZM, 12ZM,  
12ZN, 12ZN,  
12ZO, 12ZO,  
12ZP, 12ZP,  
12ZQ, 12ZQ,  
12ZR, 12ZR,  
12ZS, 12ZS,  
12ZT, 12ZT,  
12ZU, 12ZU,  
12ZV, 12ZV,  
12ZW, 12ZW,  
12ZX, 12ZX,  
12ZY, 12ZY,  
12ZZ, 12ZZ,  
12AA, 12AA,  
12AB, 12AB,  
12AC, 12AC,  
12AD, 12AD,  
12AE, 12AE,  
12AF, 12AF,  
12AG, 12AG,  
12AH, 12AH,  
12AI, 12AI,  
12AJ, 12AJ,  
12AK, 12AK,  
12AL, 12AL,  
12AM, 12AM,  
12AN, 12AN,  
12AO, 12AO,  
12AP, 12AP,  
12AQ, 12AQ,  
12AR, 12AR,  
12AS, 12AS,  
12AT, 12AT,  
12AU, 12AU,  
12AV, 12AV,  
12AW, 12AW,  
12AX, 12AX,  
12AY, 12AY,  
12AZ, 12AZ,  
12BA, 12BA,  
12BB, 12BB,  
12BC, 12BC,  
12BD, 12BD,  
12BE, 12BE,  
12BF, 12BF,  
12BG, 12BG,  
12BH, 12BH,  
12BI, 12BI,  
12BJ, 12BJ,  
12BK, 12BK,  
12BL, 12BL,  
12BM, 12BM,  
12BN, 12BN,  
12BO, 12BO,  
12BP, 12BP,  
12BQ, 12BQ,  
12BR, 12BR,  
12BS, 12BS,  
12BT, 12BT,  
12BU, 12BU,  
12BV, 12BV,  
12BW, 12BW,  
12BX, 12BX,  
12BY, 12BY,  
12BZ, 12BZ,  
12CA, 12CA,  
12CB, 12CB,  
12CC, 12CC,  
12CD, 12CD,  
12CE, 12CE,  
12CF, 12CF,  
12CG, 12CG,  
12CH, 12CH,  
12CI, 12CI,  
12CJ, 12CJ,  
12CK, 12CK,  
12CL, 12CL,  
12CM, 12CM,  
12CN, 12CN,  
12CO, 12CO,  
12CP, 12CP,  
12CQ, 12CQ,  
12CR, 12CR,  
12CS, 12CS,  
12CT, 12CT,  
12CU, 12CU,  
12CV, 12CV,  
12CW, 12CW,  
12CX, 12CX,  
12CY, 12CY,  
12CZ, 12CZ,  
12DA, 12DA,  
12DB, 12DB,  
12DC, 12DC,  
12DD, 12DD,  
12DE, 12DE,  
12DF, 12DF,  
12DG, 12DG,  
12DH, 12DH,  
12DI, 12DI,  
12DJ, 12DJ,  
12DK, 12DK,  
12DL, 12DL,  
12DM, 12DM,  
12DN, 12DN,  
12DO, 12DO,  
12DP, 12DP,  
12DQ, 12DQ,  
12DR, 12DR,  
12DS, 12DS,  
12DT, 12DT,  
12DU, 12DU,  
12DV, 12DV,  
12DW, 12DW,  
12DX, 12DX,  
12DY, 12DY,  
12DZ, 12DZ,  
12EA, 12EA,  
12EB, 12EB,  
12EC, 12EC,  
12ED, 12ED,  
12EE, 12EE,  
12EF, 12EF,  
12EG, 12EG,  
12EH, 12EH,  
12EI, 12EI,  
12EJ, 12EJ,  
12EK, 12EK,  
12EL, 12EL,  
12EM, 12EM,  
12EN, 12EN,  
12EO, 12EO,  
12EP, 12EP,  
12EQ, 12EQ,  
12ER, 12ER,  
12ES, 12ES,  
12ET, 12ET,  
12EU, 12EU,  
12EV, 12EV,  
12EW, 12EW,  
12EX, 12EX,  
12EY, 12EY,  
12EZ, 12EZ,  
12FA, 12FA,  
12FB, 12FB,  
12FC, 12FC,  
12FD, 12FD,  
12FE, 12FE,  
12FF, 12FF,  
12FG, 12FG,  
12FH, 12FH,  
12FI, 12FI,  
12FJ, 12FJ,  
12FK, 12FK,  
12FL, 12FL,  
12FM, 12FM,  
12FN, 12FN,  
12FO, 12FO,  
12FP, 12FP,  
12FQ, 12FQ,  
12FR, 12FR,  
12FS, 12FS,  
12FT, 12FT,  
12FU, 12FU,  
12FV, 12FV,  
12FW, 12FW,  
12FX, 12FX,  
12FY, 12FY,  
12FZ, 12FZ,  
12GA, 12GA,  
12GB, 12GB,  
12GC, 12GC,  
12GD, 12GD,  
12GE, 12GE,  
12GF, 12GF,  
12GG, 12GG,  
12GH, 12GH,  
12GI*

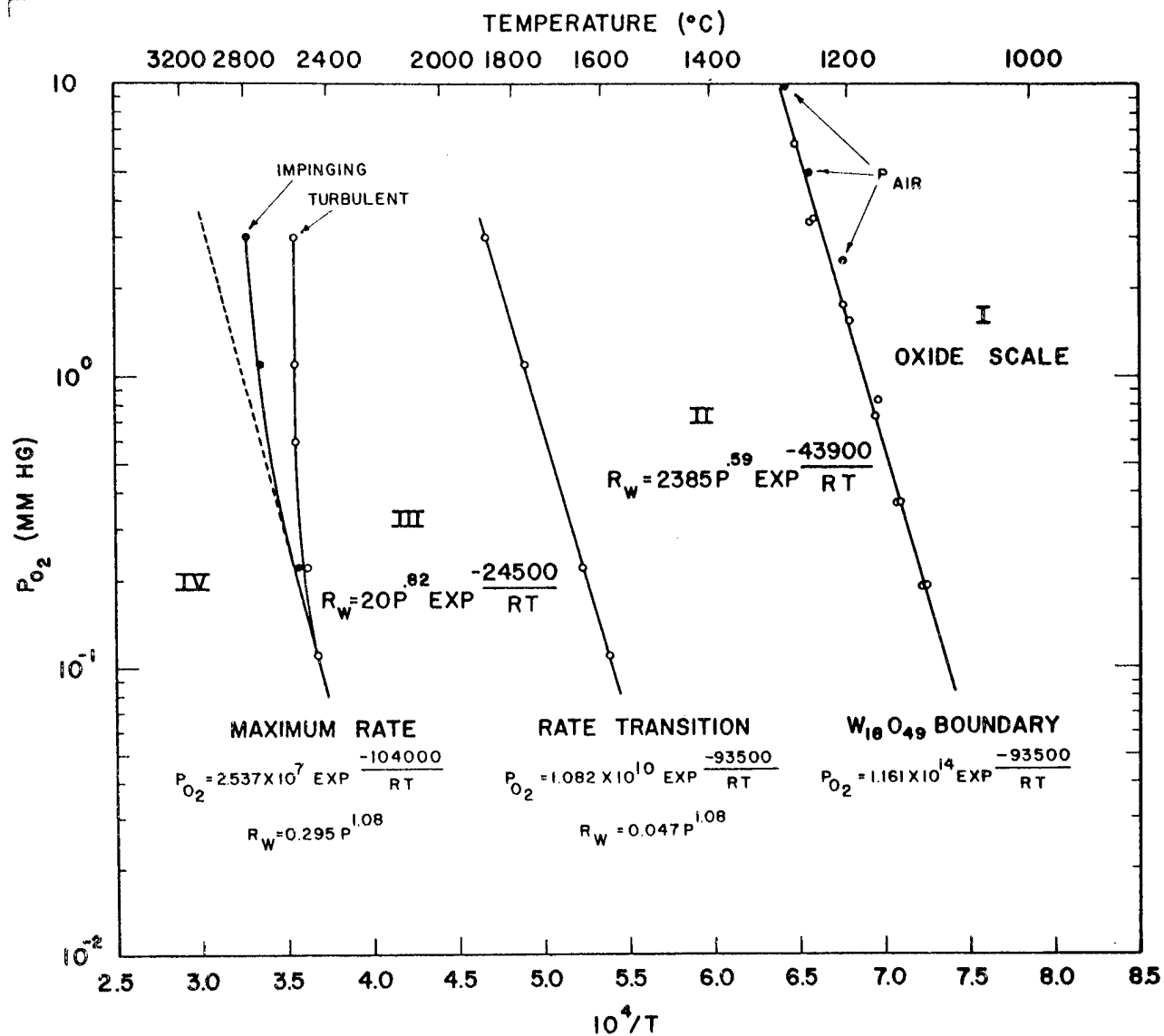


Fig. 12 Summary of Oxidation Behavior at Low Pressure and High Temperature

*end*

temperature at low pressure. Practically all other oxidation data are from tests where the gas and metal are at the same temperature. If the rate is determined by a reaction on the surface rather than by the impact of gas molecules with the surface, then the effect of gas temperature usually will be negligible. Langmuir (Ref. 2) found that reaction rate was determined by the temperature of the metal and was not affected by variations in gas temperature over a 300°K range. Additional work is needed however to prove conclusively the independence of rate on gas temperature.

The effect of dissociation of the gas before striking the surface is unknown and is a factor that should be investigated. If the heat of adsorption of oxygen is a factor in determining rates, as proposed by Becker (Ref. 4), then dissociation would have a significant effect.

## 5.1 CONCLUSIONS

- (1) The rate of oxidation of tungsten from 1,300 to 3,350°C (2,370 to 6,060°F) in air or oxygen at pressures below 5 mm Hg is equal for the same partial pressure of oxygen. Rate is a function of metal temperature, oxygen pressure, and crystal orientation.
- (2) In static or slowly moving air at all pressures and in oxygen at pressures above 3.0 mm Hg, rates may be limited by transport of oxygen to the surface. High-velocity flow is needed to provide a known and constant pressure of oxygen. When a constant oxygen pressure is maintained at the metal surface, gas velocity up to Mach 1 has no effect on the rate of reaction.
- (3) At temperatures above a boundary defined by  $P_{O_2} = 1.161 \times 10^{14} \exp. (-93,500/RT)$  a visible oxide scale does not form on tungsten in oxygen at low pressure. In air, the boundary is defined by the total pressure.
- (4) At temperatures above the oxide scale boundary, rate of metal loss is described by the relation  $R_W = 2,385 P_{O_2}^{0.59} \exp. (-43,900/RT) \text{ gm/cm}^2/\text{min.}$
- (5) A transition in rate behavior occurs at a boundary defined by  $P_{O_2} = 1.082 \times 10^{10} \exp. (-93,500/RT)$ .

At temperatures above this transition, the rate of tungsten loss is described by

$$R_W = 20 P_{O_2}^{0.82} \exp. (-24,500/RT) \text{ gm/cm}^2/\text{min}$$

- (6) The rate of oxidation reaches a maximum at a temperature defined by  $P_{O_2} = 2.537 \times 10^7 \exp. (-104,000/RT)$ . The maximum rate of metal loss at any pressure is given by the relation  $R_W = 0.295 P_{O_2}^{1.08} \text{ gm/cm}^2/\text{min}$ . At pressure above  $10^{-1}$  mm Hg, behavior near the temperature of maximum rate is influenced by gas velocity.
- (7) At temperatures above the rate maximum, the rate of metal loss increases as a linear function of oxygen pressure and decreases with temperature.
- (8) A common mechanism appears to exist in the oxidation behavior of tungsten at high temperatures in oxygen at pressures from  $10^{-6}$  to at least 10 mm Hg. The empirical rate equations in conclusions (5) and (6) above will accurately predict rates, which vary by a factor of up to 10 million in this pressure range.

Section 6  
REFERENCES

1. R. A. Perkins, L. A. Riedinger, and S. Sokolsky, "Problems in the Oxidation Protection of Refractory Metals in Aerospace Applications" (paper presented at Seventh Symposium on Ballistic Missile and Space Technology, Aug 1962)
2. I. Langmuir, "Chemical Reactions at Very Low Pressure," J. Am. Chem. Soc., Vol. 35, No. 2, 1913, p. 105
3. J. Esinger, "Adsorption of Oxygen on Tungsten," J. Chem. Phys., Vol. 30, 1959, p. 412
4. J. Becker, E. Becker, and R. Brandes, "Reactions of Oxygen with Pure Tungsten and Tungsten Containing Carbon," J. App. Phys., Vol. 32, No. 3, 1961, p. 411
5. H. Anderson, Kinetic Studies of the Reactions Occurring Between Tungsten and Gases at Low Pressure and High Temperatures, Ph. D., Thesis, University of California Lawrence Laboratory, UCRL-10135, UC-4 Chemistry, Contract No. W-7405-eng-48, Apr 1962
6. R. Perkins and D. Crooks, "Low-Pressure High-Temperature Oxidation of Tungsten," J. of Metals, Jul 1961, p. 490
7. Wright Air Development Center, Oxidation of Tungsten and Tungsten-Based Alloys, by P. Blackburn, K. Andrew, E. Gulbansen, and F. Brassart, WADC TR 59-575-II, Jun 1961
8. Ford Motor Company, Aeronutronic Division, Oxidation of Refractory Metals as a Function of Pressure, Temperature, and Time: Tungsten in Oxygen, by J. N. Ong, Research Laboratory Report, Oct 1961